Barker, P.F., Camerlenghi, A., Acton, G.D., and Ramsay, A.T.S. (Eds.)
Proceedings of the Ocean Drilling Program, Scientific Results Volume 178

36. Magnetobiochronologic Synthesis of ODP Leg 178 Rise Sediments from the Pacific Sector of the Southern Ocean: Sites 1095, 1096, and 1101[1]

Masao Iwai,[2] Gary D. Acton,[3] David Lazarus,[4] Lisa E. Osterman,[5] and Trevor Williams[6]

ABSTRACT

During Ocean Drilling Program (ODP) Leg 178, eight holes were drilled at three sites (1095, 1096, and 1101) on the continental rise along the western Antarctic Peninsula. The rise sediments proved to be good paleomagnetic recorders and provided continuous magnetostratigraphic records at all three sites. Biosiliceous microfossils, particularly diatoms and radiolarians, were present in the upper Miocene through lower Pliocene sections. In the upper Pliocene to Pleistocene sections, biosiliceous microfossils were rare but calcareous nannofossils and foraminifers were present. This paper summarizes the biostratigraphy and magnetostratigraphy of Leg 178 continental rise sites and is the first attempt at direct calibration of Antarctic biostratigraphic events to the geomagnetic polarity timescale in the Pacific sector of the Southern Ocean.

INTRODUCTION

The principal objectives of Ocean Drilling Program (ODP) Leg 178 were (1) to extract and compare high-resolution records of the past 10 m.y. of continental glaciation of the Antarctic Peninsula Pacific margin contained in topset and foreset beds (paleoshelf) of the same sequence

[1]Iwai, M., Acton, G.D., Lazarus, D., Osterman, L.E., and Williams, T., 2002. Magnetobiochronologic synthesis of ODP Leg 178 rise sediments from the Pacific sector of the Southern Ocean: Sites 1095, 1096, and 1101. *In* Barker, P.F., Camerlenghi, A., Acton, G.D., and Ramsay, A.T.S. (Eds.), *Proc. ODP, Sci. Results,* 178, 1–40 [Online]. Available from World Wide Web: <http://www-odp.tamu.edu/publications/178_SR/VOLUME/CHAPTERS/SR178_36.PDF>. [Cited YYYY-MM-DD]
[2]Department of Natural Environmental Science, Kochi University, Kochi 780-8520, Japan. iwaim@cc.kochi-u.ac.jp
[3]Ocean Drilling Program, Texas A&M University, 1000 Discovery Drive, College Station TX 77845-9547, USA.
[4]Palaeontologische Institüt, Museum fuer Naturkunde, Invalidenstrasse 43, D-10115 Berlin, Germany.
[5]U.S. Geological Survey, MS 926A, Reston VA 20192, USA.
[6]Borehole Research Group, Lamont-Doherty Earth Observatory of Columbia University, PO Box 1000, 61 Route 9W, Palisades NY 10964, USA.

Initial receipt: 15 November 2001
Acceptance: 1 August 2002
Web publication: 6 November 2002
Ms 178SR-236

of a glacial prograded wedge and in the hemipelagic sediment drifts on the continental rise; (2) to compile a high-resolution history of grounded ice volume fluctuations and compare it with low-latitude records of sea level change and isotopic estimates of ice volume change over the past 10 m.y.; and (3) to assess the main controls on sediment transport and deposition during glacial intervals and use the insights gained to optimize investigation of the longer, more complicated East Antarctic record of glaciation and glacioeustatic sea level change (Barker, Camerlenghi, Acton, et al., 1999).

More than two decades ago, four sites were drilled on the Bellingshausen Abyssal Plain (Sites 322 and 323) and continental rise (Sites 324 and 325) off the West Antarctic Peninsula (Hollister, Craddock, et al., 1976) during Deep Sea Drilling Project (DSDP) Leg 35. Ice-rafted debris was first recorded in lower to middle Miocene sediments at Site 325 (Hollister, Craddock, et al., 1976). However, poor core recovery at Leg 35 sites limited the glacial and paleoceanographic interpretations that could be made (Barker, Camerlenghi, Acton, et al. 1999). Early drilling on the Antarctic rise and shelf had varying success. DSDP Leg 28 had good core recovery in most holes drilled, with the exception of Site 271 (recovery = 8%), which had difficulty coring through glacial till. ODP Southern Ocean cruises (Legs 113, 114, 119, 120, and 177) greatly improved regional biostratigraphic knowledge (e.g,. Gersonde et al., 1990; Thomas et al., 1990; Barron et al., 1991; Harwood et al., 1992; Gersonde and Barcena, 1998). Although these drilling legs developed biostratigraphy in an open-ocean environment, the resultant diatom zonations (and presumably those of other microfossil groups) are also mostly applicable to the Ross Sea Shelf environment (Winter and Harwood, 1997).

ODP Leg 178 returned to this region in order to refine our understanding of late Neogene West Antarctic Ice Sheet history (Barker and Camerlenghi, 1999). Three sites on the continental rise (Sites 1095, 1096, and 1101) and four sites on the continental shelf (Sites 1097, 1100, 1102, and 1103) were drilled during Leg 178 (Fig. **F1;** Table **T1**). Late Miocene to Holocene glacial and interglacial sediments were recovered at the rise and drift sites drilled during Leg 178 (Sites 1095, 1096, and 1101). The upper Quaternary sections of all three sites contained a rare and sporadic record of biosiliceous microfossils with reworked species, a result consistent with other cores taken from around the Antarctic continent. Even though the upper Quaternary assemblage is often sparse, a biostratigraphic signal is obvious. Preservation in general was better in pre-Quaternary parts of the drilled sections, where many samples yielded well-preserved and diverse microfossil assemblages.

Shipboard work was conducted using the magnetochronological calibrations of Berggren et al. (1995). The biochronological framework used during Leg 178 follows that established during ODP Legs 119 (Barron et al., 1991) and 120 (Harwood et al., 1992). The strategy was to establish a biochronological framework at the rise sites and apply it to the shelf sites to investigate the glacial history of Antarctica (Barker, Camerlenghi, Acton, et al., 1999). Here, we link together the multiple stratigraphic and geochronological efforts that have been devoted to Leg 178 sediments, with revised species datum depths and ages as well as data charts for each site. Detailed descriptions of the biostratigraphy of Leg 178 sites are given elsewhere: diatoms of rise sites (Winter and Iwai, **Chap. 29,** this volume), quantitative diatoms of Site 1095 (Iwai, 2000a, 2000b, 2001, unpubl. data), radiolarians of Hole 1095B (Lazarus, **Chap. 13,** this volume), nannofossils of Sites 1096 and 1101 (Winter and

F1. Location of ODP Leg 178 sites, p. 20.

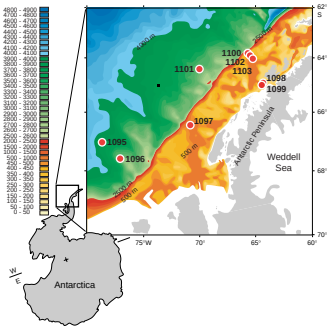

T1. Holes cored during Leg 178, p. 29.

Wise, **Chap. 26,** this volume), and nannofossils of Site 1095 (Kameo in Iwai et al., **Chap. 28,** this volume).

The preliminary magnetostratigraphy proposed for the rise sites during Leg 178 (Barker, Camerlenghi, Acton, et al., 1999) has been revised by Acton et al. (**Chap. 37,** this volume). Details of the differences in interpretations are discussed in their paper. In essence, their revisions were based primarily on a large number of paleomagnetic observations from U-channel samples and the use of composite depth scales, along with the reevaluation of shipboard data in light of these new constraints. In addition, Acton et al. (**Chap. 37,** this volume) incorporated the revised biostratigraphic events and datums from this study. Similarly, Williams et al. (**Chap. 31,** this volume) present a revised interpretation of the magnetic logging data from Sites 1095 and 1096, which is consistent with that from the paleomagnetic measurements on core material. Thus, the paleomagnetic, magnetic logging, and biostratigraphic data from this paper and those of Acton et al. (**Chap. 37,** this volume) and Williams et al. (**Chap. 31,** this volume) present a coherent and consistent interpretation of the chronostratigraphy for the Neogene sedimentary sections.

MAGNETOBIOCHRONOLOGIC FRAMEWORK

We tie our Leg 178 biochronology to the geomagnetic polarity timescale (GPTS) of Berggren et al. (1995) (BKSA95), which uses the GPTS of Cande and Kent (1995) (CK95). BKSA95 use the astronomically calibrated timescale for polarity boundaries from Chron 1n to Subchron 3n.4n (0–5.23 Ma) (Shackleton et al., 1990; Hilgen, 1991a, 1991b). Extension of the astronomical timescale into the Miocene epoch (Shackleton et al., 1995 [Leg 138]; Shipboard Scientific Party, 1995 [Leg 154]) and fine-tuning of the chronology of the astronomical timescale (e.g., Langereis et al., 1994) is an ongoing process. The differences between astronomical and geomagnetic timescales are <0.25 m.y. for the time interval between the late Miocene and the Quaternary.

For this paper absolute microfossil datum ages are from BKSA95 or were converted from published age estimates based on Berggren et al. (1985a, 1985b) to the timescale of Cande and Kent (1995) through linear interpolation between the nearest geomagnetic reversal boundaries. The biostratigraphic zonation for different groups employed on Leg 178 sediments are summarized in Figure **F2.** Sources of biostratigraphic ages (Table **T2**) are as follows.

Diatoms

Numerous diatom biostratigraphic studies have been completed for the Southern Ocean (Gersonde and Burckle, 1990; Baldauf and Barron, 1991; Harwood and Maruyama, 1992; Gersonde and Barcena, 1998; Gersonde, Hodell, Blum, et al., 1999; Ramsay and Baldauf, 1999). The Neogene and Quaternary diatom zonal scheme used during Leg 178 was that proposed by Harwood and Maruyama (1992 [Leg 120]) with the modifications of Winter and Iwai (**Chap. 29,** this volume) and Iwai (2000a, 2000b).

Abundance and state of preservation vary greatly within Leg 178 sites, with intervals of rare siliceous microfossils noted in the middle Pliocene and Pleistocene. Taxonomic concepts for diatoms from Leg

F2. Summary of the Neogene chronostratigraphy, p. 21.

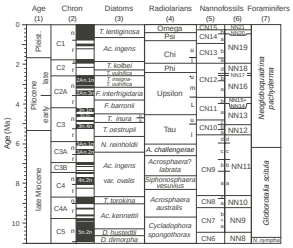

T2. Ages of biostratigraphic events, p. 30.

178 sediments are discussed in Iwai and Winter (**Chap. 35,** this volume).

Radiolarians

Radiolarians were initially studied by Weinheimer during the Leg 178 cruise (Barker, Camerlenghi, Acton et al., 1999). More detailed analyses of the upper Miocene to lower Pliocene interval between 4 and 9 Ma (98 samples from Cores 178-1095B-5H through 52X) were completed by Lazarus (**Chap. 13,** this volume).

The radiolarian biostratigraphic scheme proposed by Lazarus (1990, 1992) was applied to Leg 178 material. This zonation is based on the earlier schemes of Hays (1965), Chen (1975), Weaver (1976), Keany (1979), and Caulet (1991) and refined by Lazarus (1992) using sediments recovered during Legs 119 and 120. Species concepts follow those used by Keany (1979), Lazarus (1990, 1992), and references therein. Stratigraphic constraints of radiolarian events are based on examination of one sample per core (core catcher) for Sites 1096 and 1101 and two to four samples per core for Site 1095 (Lazarus, **Chap. 13,** this volume).

Calcareous Nannofossils

The abundance of calcareous nannofossils is generally low throughout the section of all three rise sites, except in the Pleistocene–late Pliocene biocalcareous interval of Sites 1096 and 1101 (Shipboard Scientific Party, 1999a). Remarks regarding the biostratigraphic zonations and calcareous nannofossil datums used in this paper can be found in Winter and Wise (**Chap. 26,** this volume) for Sites 1096 and 1101 and in Iwai et al. (**Chap. 28,** this volume) for Site 1095 and continental shelf sites.

The zonal schemes used for Leg 178 were those of Martini (1971) and Bukry (1973, 1975, 1978), code numbered by Okada and Bukry (1980). In addition to the traditional use of first/last occurrences of index species, ranges of other taxa were used to improve the stratigraphic resolution of the Pleistocene–late Pliocene interval (Thierstein et al., 1977; Gartner, 1977, 1990; Pujos, 1988; Raffi et al., 1993; Wei, 1993; Takayama and Sato, 1987; Raffi and Flores, 1995).

Foraminifers

Several zonal schemes have been developed for the mid and high latitudes of the Southern Hemisphere (e.g., Jenkins and Srinivasan, 1986; Berggren et al., 1995). However, these schemes are not fully applicable to the planktonic foraminiferal fauna in all the sediments recovered during Leg 178 because of the absence or low abundance of foraminiferal species. In general, high-latitude foraminiferal assemblages contain low-diversity and long-ranging species that are of limited biostratigraphic use. Planktonic foraminiferal zonation and classification follow Berggren (1992), developed from Leg 120 Sites.

Magnetostratigraphy

The polarity zones recorded in the drift sediments can be correlated to the GPTS with little or no ambiguity, particularly for Sites 1096 and 1101, as discussed in the revised magnetostratigraphic interpretations

of Acton et al. (**Chap. 37,** this volume). As noted in the introduction, Acton et al. (**Chap. 37,** this volume) make use of the revised biostratigraphic events and datums from this study, resulting in an internally consistent interpretation for the biomagnetostratigraphy. They suggest that neither hiatuses nor abrupt large changes in sedimentation rates are needed to match the polarity zones to the GPTS, although such an interpretation gives rise to discrepancies in the biostratigraphic datums for part of the Site 1095 sedimentary section.

The discrepancies may arise for several reasons (see also **"Synthesis and Discussion,"** p. 11), some of which may be related to magnetostratigraphy from Leg 178 or previous drilling. In particular, biostratigraphic datums may have been miscorrelated with the GPTS in prior studies owing to incomplete recovery, hiatuses, and sediments that are less than ideal paleomagnetic recorders, all of which can lead to inaccurate magnetostratigraphies. Such problems could also affect the Leg 178 sites. Thus, we also investigate an alternate interpretation of the paleomagnetic data for Site 1095, which includes a hiatus near the Miocene/Pliocene boundary.

Depth Scales

Depths are given in meters below seafloor (mbsf), which is based on drill pipe measurements specific to each drill hole, and, when necessary, in meters composite depth (mcd), which is a depth scale common to all holes at a site. The mcd scale overcomes some of the inaccuracies in the mbsf scale, but more importantly, allows coeval stratigraphic features recovered in more than one hole to be placed at a common depth (e.g., Barker, **Chap. 6,** this volume). Such features could be misaligned in depth by several meters in the mbsf depth scale as illustrated for polarity reversals in Figure **F12,** p. 33, of Acton et al. (**Chap. 37,** this volume).

We use the mcd scales for Sites 1095 and 1096 constructed by Barker (**Chap. 6,** this volume). Using tables in his paper, the mbsf depth can be converted to mcd by adding or subtracting the appropriate offset in meters. The offsets vary in the upper part of Sites 1095 and 1096. Because the deeper portions of both sites are single cored, a constant offset is used for most of the section. For example, at Site 1095, only Hole 1095B was cored below ~90 mbsf. Thus, below the top of Core 178-1095B-2H at 92.5 mbsf, a constant offset of –5.5 m is applied to obtain mcd depths (e.g., 92.5 mbsf = 87.0 mcd). Similarly, only Hole 1096C was cored below ~260 mbsf. Thus, below the top of Core 178-1096C-8X at 260.9 mbsf, a constant offset of +5.54 m is applied to obtain mcd depths. Finally, no mcd scale is needed for Site 1101 because only a single hole (1101A) was cored. All depths for Site 1101 are therefore given in mbsf only.

Offsets also occur between depths from wireline measurements made during downhole logging and the drill pipe measurements. For Hole 1095B, Acton et al. (**Chap. 37,** this volume) determined the offsets by correlating whole-core susceptibility with susceptibility measured on the second logging run of the Geologic High-Resolution Magnetic Tool (GHMT). The depth offsets between whole-core susceptibility events and logging events are fairly constant, with the logging depths being on average 4 to 6 m deeper than mbsf depths and 9 to 11 m deeper than mcd depths.

DATA SOURCES: MAGNETOBIOCHRONOLOGY OF LEG 178 RISE SITES

All published and unpublished biostratigraphic results have been compiled into tables showing first or last occurrences of biostratigraphic marker species (Tables T3, T4, T5). This data, together with the interpreted paleomagnetic polarity pattern, is shown in downhole log format for each Site in Figures F3, F4, and F5 and graphically as age-depth plots (Figs. F6, F7, F8). There is a disagreement between the biostratigraphy of biosiliceous fossils and the magnetostratigraphy at Site 1095. Iwai (2000a, 2000b) noted the possibility of a Miocene–Pliocene hiatus at this site. Table T6 summarizes the magnetic anomaly correlatives identified in the Leg 178 *Initial Reports* volume (Barker, Camerlenghi, Acton, et al., 1999) and the alternative postcruise correlation by Iwai (2000a, 2000b).

Site 1095

Site 1095 (66°59.1′S, 78°29.3′W; 3842 m water depth) is located on the continental rise along the Pacific margin of the Antarctic Peninsula. A sedimentary section, 570 m thick, extending from the Holocene to the upper Miocene (~9.6 Ma), was recovered from a hemipelagic sediment drift (Rebesco et al., 1997) (Fig. F1). Drilling at Site 1095 was targeted to recover an older part of the sedimentary section than at Site 1096 to extend the studies of the history of glaciation back in time. Four holes (1095A–1095D) were drilled (Barker, Camerlenghi, Acton, et al., 1999). Recovery was generally excellent (average recovery = 89% for the entire hole), although there is a short interval from 209.2 to 228.4 mcd (Cores 178-1095B-15X and 16X) where recovery was <50%, a gap resulting from zero recovery in Core 178-1095B-19X at 247.6–257.2 mcd, and poor recovery in the basal cores of Hole 1095B (Cores 178-1095B-43X through 52X).

The recovered sediments are mostly diatomaceous silty clays derived from distal turbidite, contourite, and hemipelagic sedimentation (Barker, Camerlenghi, Acton, et al., 1999). The uppermost 50 m consists of laminated and massive, often extensively bioturbated, diatom-bearing silty clays (Unit I). These deposits show a marked cyclic pattern of alternating gray, terrigenous, and brown biogenic-rich silty clays, which are the stratigraphic expression of successive glacial and interglacial cycles. Lithostratigraphic Unit II extends from 46.0 mcd down to 429.5 mcd and consists mainly of green laminated silts and muds. Sediments below 429.5 mcd (Unit III) consist of nonbioturbated parallel-laminated siltstone-claystones with sporadic occurrences of diatomaceous claystone. This facies of Unit III does not show the cyclic pattern observed in overlying sediments. One possible Pleistocene hiatus was suggested at ~56 mcd (~60 mbsf) (Acton et al., Chap. 37, this volume).

Biostratigraphic Summary

The stratigraphic position of microfossil zonal boundaries at Site 1095 is shown in Tables T3 and T5 and in Figure F3. Diatoms and radiolarians provide the majority of age constraints for Site 1095. Diatoms are common in the upper Miocene to lower Pliocene section and are rare and sporadic in the upper Pliocene through Quaternary section

T3. Constraints of biostratigraphic events from continental rise sites, p. 32.

T4. Depths of biostratigraphic events at Site 1095, p. 34.

T5. Depths of biostratigraphic events at Sites 1096 and 1101, p. 35.

F3. Magnetostratigraphic and biostratigraphic summary of Site 1095, p. 22.

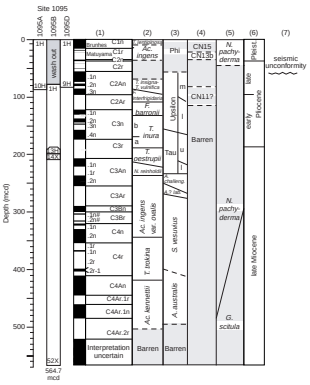

F4. Magnetostratigraphic and biostratigraphic summary of Site 1096, p. 23.

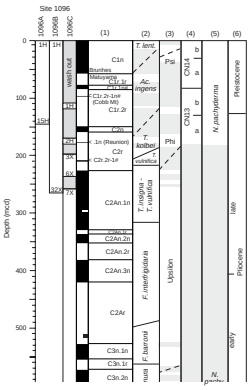

F5. Magnetostratigraphic and biostratigraphic summary of Site 1101, p. 24.

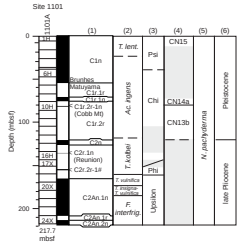

from Cores 178-1095A-1H through 9H and below Core 178-1095B-46X (>498 mcd; >9.4 Ma).

The diatom biostratigraphy of Holes 1095A, 1095B, and 1095C is complex and contains an incomplete record of Pleistocene through upper Miocene datums and events. The Pliocene to Pleistocene is contained in glacial and interglacial hemipelagic sediments, whereas the Miocene consists mainly of turbidites. Many core intervals are barren or have a low abundance and diversity of diatomaceous material. In samples that have diatoms, reworking of older species is often noted. In spite of the obvious reworking, there is a strong biostratigraphic signal for the early Pliocene and late Miocene. Material used in the biostratigraphic analysis of this site was taken from the core catchers and within the split cores (usually one sample per section).

The samples in Cores 178-1095B-29X through 45X contained a typical late Miocene diatom assemblage, with a large proportion of *Denticulopsis* species dominating. The species of *Denticulopsis* that are used as zonal boundary markers in older sediments, *D. dimorpha* and *D. praedimorpha,* were absent from the assemblage. One sieved sample from Core 178-1095B-37X contained *Asteromphalus kennetii,* which has a first occurrence age of 10.29 Ma. This datum also helps constrain the age of the lower part of Hole 1095B to the late Miocene.

All previously defined standard radiolarian zones for the late Miocene to earliest Pliocene can be identified in Hole 1095B between 180 and 460 mcd, including the basal Tau, *A. challengerae, A. labrata, S. vesuvius,* and upper *A. australis* Zones of Lazarus (1992). As noted, however, by Lazarus (**Chap. 13,** this volume), radiolarian occurrences are sporadic and the placement of zonal boundaries are thus somewhat imprecise.

The biostratigraphy of calcareous nannofossils in material from Site 1095 is also discontinuous and incomplete but provides biostratigraphic age control in the upper intervals of the site. *Emiliania huxleyi*, whose appearance defines the base of the calcareous nannofossil Zone CN15 (Okada and Bukry, 1980), is found only in Sample 178-1095A-1H-2, 70 cm (2.16 mcd). Samples 178-1095A-3H-5, 18.5 cm, through 5H-1, 90 cm (15.44–27.79 mcd), mostly contain *Pseudoemiliania lacunosa* without *E. huxleyi*. It suggests that this interval is assigned to Zone CN13.

Magnetostratigraphic Summary

Paleomagnetic results from Site 1095 provide a magnetostratigraphy that correlates well with the GPTS from the termination of Chron C4Ar.2n (9.580 Ma) at ~510 mcd up to the Brunhes Chron (Table **T7;** Fig. **F3**). Exceptions occur in a few intervals where core deformation, dropstones, magnetic overprints, or low recovery bias or obscure the paleomagnetic signal, as discussed below.

The initial interpretation of the shipboard paleomagnetic data was difficult for the upper 100 m of the section owing to conflicting results from Holes 1095A and 1095D. This was due mainly to depth offsets that occur in the mbsf depth scales, which were overcome by using the mcd depth scale (Barker, **Chap. 6,** this volume), and to paleomagnetic overprints. Even with more detailed stepwise demagnetization of U-channel samples, Acton et al. (**Chap. 37,** this volume) observed that the interval from 17 to 55 mcd is more complexly magnetized than intervals above or below. As a result, none of the short polarity intervals occurring in the past 2.5 m.y., including the Jaramillo Subchron

F6. Age-depth profile at Site 1095, p. 25.

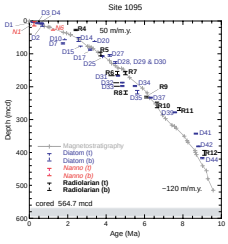

F7. Age-depth profile at Site 1096, p. 26.

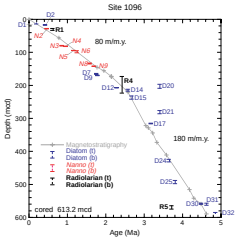

F8. Age-depth profile at Site 1101, p. 27.

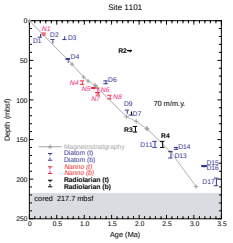

T6. Previous magnetostratigraphic interpretations for Site 1095, p. 37.

T7. Summary of magnetostratigraphy at Sites 1095, 1096, and 1101, p. 38.

(Subchron C1r.1n), the Cobb Mountain Event (Cryptochron C1r.2r-1n), the Reunion Event (Subchron C2r.1n), and Cryptochron C2r.2r-1n can be confidently identified. Within the complexly magnetized interval, Acton et al. (**Chap. 37,** this volume) interpret the normal polarity zone from 34.68 to 37.33 mcd as Chron C2n, which places the termination of Chron C2n about 20 m above the depth given by the Shipboard Scientific Party (1999b). (In the interpretation of the Shipboard Scientific Party [1999b], all reversals from the termination of Chron C2n to the onset of C2An.1n were lost in a hiatus).

Downhole magnetic logging with the GHMT was able to provide a complete polarity stratigraphy to the base of Hole 1095B, allowing the paleomagnetic polarities from core measurements to be extended into the interval of low core recovery below ~474.5 mcd. The interval from 485.5 to 517.5 mcd is dominantly of reversed polarity, whereas below 517.5 mcd to the base of the logs (551 mcd) it is of normal polarity, with the exception of two or three shorter reversed polarity events.

Variations in the remanent anomaly signal calculated from data collected on the second pass of the GHMT logging tool in Hole 1095B (Williams et al., **Chap. 31,** this volume) mimic the variations in the paleomagnetic inclination signal from the cores from Hole 1095B (Fig. **F9**). In this comparison, we have transformed the remanent anomaly signal, which was in the logging depth scale, to the mcd scale using Table **T16,** p. 61, from Acton et al., (**Chap. 37,** this volume). The depth conversion uses linear interpolation between the published tie points. The remanent anomaly data in mcd, mbsf, and logging depth scales are included in Table **T8** along with the full data set from the GHMT logging tool. The geomagnetic reversals, which are evidenced by a change in the sign of the inclination and remanent anomaly signals, correlate well as do the more subtle variations in the signals within intervals of constant polarity. Thus, the paleomagnetic data and magnetic logging data give a consistent magnetostratigraphy for Site 1095.

The magnetostratigraphy proposed by Acton et al. (**Chap. 37,** this volume) results in sedimentation rates that vary from 10 to 114 m/m.y., with the exception of the normal polarity zone from 455.37 to 480.03 mcd, interpreted to be Chron 4Ar.1n (9.230–9.308 Ma), over which the sedimentation rate is 316 m/m.y. Overall, the sedimentation rate increases progressively downhole, so a higher rate near the base of the section where Chron 4Ar.1n is located may not be exceptional. Below 480 mcd, the magnetostratigraphy becomes uncertain owing to poor core recovery. Both the core measurements and the magnetic logging data indicate that a reversed polarity zone is present from 480.3 to ~515 mcd, which we interpret to be Chron C4Ar.2r. A normal polarity zone appears to extend from ~515 mcd to the base of the hole, which could represent Chron C4Ar.2n or some combination of Chrons C4Ar.2n through C5n.2n.

Site 1096

Site 1096 (67°34.0′S, 76°57.8′W; 3152 m water depth) was drilled near the crest of a hemipelagic sediment drift on the continental rise off the northwest Pacific margin of the Antarctic Peninsula; a more proximal, shallower location than Site 1095 (Fig. **F1**). Site 1096 was drilled in order to obtain the shallower part of the stratigraphic section, where it is most expanded. At this site we recovered a complete double advanced hydraulic piston corer (APC) section to ~140 mcd and an extended core

F9. The magnetostratigraphy of Site 1095, p. 28.

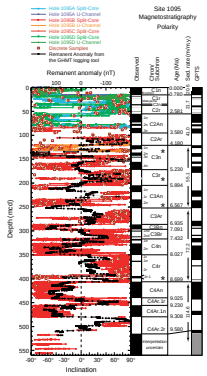

T8. GHMT downhole magnetic logging data, p. 40.

barrel (XCB) cored section to 613.2 mcd, and the site was logged using multiple downhole tools.

The sediments recovered are predominantly fine grained and terrigenous, consistent with drift deposition, and are divided into three depositional units. A detailed lithologic description is given in the "Site 1096" chapter of the Leg 178 *Initial Reports* volume (Shipboard Scientific Party, 1999c). The age of the sediments extends from the Holocene to the early Pliocene.

Biostratigraphic Summary

The stratigraphic position of microfossil zonal boundaries at Site 1096 is presented in Tables **T3** and **T5** and in Figure **F4.**

Site 1096 has better-preserved microfossils than Site 1095. Above 175 mcd (Units I and II) the sediments contain calcareous nannofossils and foraminifers. Below this depth, the biostratigraphy is based on the biogenic silica record. In the upper 110 m of Hole 1096A and the upper parts of Holes 1096B and 1096C, diatoms are rare or absent and the diatom zonal boundary markers are not seen. The exception to this is noted in brown-colored, possibly interglacial sediments present in the lower part of Cores 178-1096A-2H and 178-1096B-2H and 3H in which diatoms are common and the assemblage is dominated by *Fragilariopsis kerguelensis, Hemidiscus karstenii, Thalassionema* spp., and *Thalassiothrix* spp. fragments. Samples studied from 115 to 170 mcd are barren of diatoms. From 175 to 613 mcd (Unit III), siliceous microfossils dominate. The diatom record for this interval is virtually complete, with zonal datums being available for nearly all the zones. The record of radiolarians is relatively complete for Unit III, and most of the marker species are present through the entire Upsilon Zone. Radiolarians are present in several intervals, but the marker species for the two zones below Psi (Chi and Phi) were not found. Foraminifers are rare to abundant only in the upper interval of Site 1096. *Neogloboquadrina pachyderma* sinistral dominates the planktonic foraminiferal assemblage and is found to the base of the hole. Benthic foraminifers are rare and consist mostly of shallow-water species presumed to be reworked from the continental shelf. The calcareous nannofossil biostratigraphy of Site 1096 is discontinuous and incomplete but provides biostratigraphic age control in the upper 175 m the section.

Magnetostratigraphic Summary

The paleomagnetic results from Site 1096 provide a magnetostratigraphy that correlates well with the GPTS from the onset of Chron C3n.2n (4.6 Ma) at ~489.68 mcd up to the Brunhes Chron (Table **T7;** Fig. **F4**). As at Site 1095, there are a few intervals where core deformation, dropstones, magnetic overprints, or low recovery obscure the paleomagnetic signal, as discussed below. Coring gaps in the double-APC cored section above ~140 mcd are negligible (Holes 1096A and 1096B). Below this, gaps of several meters may be present between cores, with potential loss of some shorter polarity zones. Also, as at Site 1095, the interval from below the Brunhes/Matuyama reversal to just above Chron C2An.1n, spanning roughly 0.8 to 2.4 Ma, has the most complex magnetization and is the most difficult to interpret.

The most significant changes to the magnetostratigraphy of Site 1096 proposed by Acton et al. (**Chap. 37,** this volume) are the identification of Chron C2n, Subchron C2r.1n (the Reunion Subchron), the

onset of Chron C2An.1n, and Chron C2An.2n. The relative stratigraphic locations of these newly identified polarity chrons and subchrons (Fig. F7) are compatible with the broader magnetostratigraphic framework completed during Leg 178 (table T21 from Shipboard Scientific Party, 1999c).

Site 1101

Site 1101 (64°22.3′S, 70°15.7°W) was drilled in 3278 m water depth, centrally located within a sediment drift ~500 km northeast of Sites 1095 and 1096.

A single hole (1101A) was APC cored to 142.7 mbsf and extended by XCB drilling to 217.7 mbsf (recovery = 99.1%). Recovered sediments consist mainly of hemipelagic clayey silt that contains a nearly continuous distal glacial record of the past 3.1 to 3.4 m.y. (late Pliocene to present). Unit I (0–53.3 mbsf) and Unit II (53.3–142.7 mbsf) are composed of alternating biogenic-bearing massive clayey silts and laminated clayey silts (Shipboard Scientific Party, 1999d).

Biostratigraphic Summary

All four microfossil groups (diatoms, radiolarians, calcareous nannofossils, and foraminifers) are present in Hole 1101A. The stratigraphic positions of microfossil zonal boundaries in Hole 1101A are given in Tables T3 and T5 and in Figure F5.

Diatom preservation and abundance varied throughout Hole 1101A. Fragmentation of valves is common throughout the upper 160 m, and diatoms in samples below Core 178-1101A-19X were more abundant than in the upper part of the hole. The lowest three cores (178-1101A-22X, 23X, and 24X) contain a diverse assemblage of open-marine diatoms. All diatom zones from the Pleistocene to the late Pliocene were identified at Site 1101.

Radiolarians were generally abundant and moderately preserved, with only two barren intervals. The Psi through Upsilon Zones (Pleistocene–Pliocene) were recovered (Fig. F5).

Calcareous microfossils were found in the uppermost core as well as in carbonate-rich intervals between 50 and 134 mbsf (Unit II). Several planktonic foraminiferal oozes were identified, mostly in Unit II. Over 90% of the individual specimens in these assemblages are *Neogloboquadrina pachyderma* sinistral, with rare *N. pachyderma* dextral, *Globigerina bulloides,* and benthic foraminifers. The carbonate-rich interval appears to be coeval with a similar interval at Site 1096.

Calcareous nannofossils were recovered in the upper 1 m. The first and last occurrence of the large form of *Gephyrocapsa* spp. was observed, making the nannofossil record at Site 1101 more complete than that at Site 1096.

Magnetostratigraphic Summary

The paleomagnetic polarity pattern from Site 1101 correlates well with the GPTS from the onset of Chron C2An.1n (3.040 Ma) at ~9.38 mbsf up to the Brunhes Chron (Table T7; Fig. F5). As at the other Leg 178 sites, exceptions occur in a few intervals where core deformation, dropstones, overprints, or low recovery obscure the paleomagnetic signal. Unlike these other sites, Site 1101, however, was cored with a single

hole. Thus, several large coring gaps that occur in the upper 60 m are not filled by core recovered at other holes.

The revised magnetostratigraphy of Acton et al. (**Chap. 37,** this volume) is virtually unchanged from that completed during Leg 178 (see table T21 and associated discussion from Shipboard Scientific Party, 1999d). Slight adjustments made were based mainly on the higher resolution of the U-channel measurements. Acton et al. (**Chap. 37,** this volume) also defined the boundaries for Subchron C1r.2r-1n (Cobb Mountain Subchron) and Subchron C2r.1n (Reunion Event), which were discussed by Shipboard Scientific Party (1999d) but not included in their table T21. The identification of both of these subchrons is speculative given the short intervals over which they occur and the level of drilling disturbance that affects some intervals cored in Hole 1101A.

SYNTHESIS AND DISCUSSION

Age-depth plots for each site are presented with magnetostratigraphic and biostratigraphic events in Figures **F6, F7,** and **F8.** Biostratigraphic data is from Tables **T4** and **T5;** polarity events and their interpretation are from Table **T7.** Previous magnetopolarity interpretations are also given in Table **T6.**

Site 1095

Miocene and Pliocene

The age model for the lowermost part of the section at Site 1095 is based solely on paleomagnetic data. Magnetostratigraphy suggests an essentially complete section throughout this time interval with high but gradually decreasing sedimentation rates (average = 80 m/m.y, with higher values of ~120 m/m.y. at the base of the section), and with only minor short-term changes in sedimentation rate values. In the interval between ~150 and 420 mcd, the biostratigraphic data, despite the presence of virtually all zones for both diatoms and radiolarians (see **"Biostratigraphic Summary,"** p. 6, in "Site 1095"), suggests significant differences in sedimentation rates, with somewhat higher rates of sedimentation on average than those implied by the magnetostratigraphic data and with the presence of an ~1-m.y.-long interval of low sedimentation, or a hiatus, at ~235 mcd. The biostratigraphic data is internally in good agreement; there is little scatter in the data, and there are not any systematic differences in age estimates between diatoms and radiolarians. Thus, whereas the age estimates from magnetostratigraphy and biostratigraphy are in broad agreement—both suggest ages from early late Miocene to basal Pliocene—there are significant offsets between the two types of data over much of the interval. The maximum age difference is ~1 m.y. in the Miocene/Pliocene boundary interval between ~215 and 275 mcd. There are several possible reasons for this discrepancy, including incorrect assignment of the paleomagnetic polarity data to the GPTS, inaccurate identification of the position of biostratigraphic events within the section, and incorrect calibrations of biostratigraphic events to the GPTS.

The magnetostratigraphic polarity pattern of Site 1095 is based on a coherent set of shipboard core measurements, U-channel samples, and logging results, and the proposed correlation in the pattern seen in the data and the GPTS, as plotted in Figure **F6,** is remarkably clear and

straightforward. Although it is possible to correlate the magnetostratigraphic polarity pattern to the GPTS in such a way that the line of correlation is in agreement with the biostratigraphic data (e.g., Iwai, 2000a, 2000b) (Table T6), such interpretations require repeated major changes in sedimentation rates within the section. There is no evidence, however, from either seismic stratigraphy or sedimentology for a hiatus in this section or for any major changes in sediment characteristics that would suggest such rapid changes in sedimentation rate.

Biostratigraphic events can be mislocated within sedimentary sections for a variety of reasons, including reworking of older specimens into younger sediments, downcore contamination of older sediments by younger sediments during drilling, range truncation due to poor preservation, extension or truncation of local ranges due to local environmental conditions, and misidentification of species due to taxonomic problems, among others. We cannot rule out such processes entirely. Indeed, given the rather sporadic nature of microfossil preservation at this site, some degree of range error from this processes is to be expected. We nonetheless note that on the whole, the biostratigraphic data is remarkably internally consistent; there is very little scatter in the data. Instead, the data is consistently offset from the age implied by the magnetostratigraphic data. It is difficult to envisage how any of the above-mentioned processes could produce so consistent a pattern of offsets in the biostratigraphic data. Nor is there any evidence that any of the other above processes was particularly important at this site: reworking has not been noted as a problem in any of the original biostratigraphic reports; samples taken from within split cores are the primary source of data in this study and, in any case, do not differ from core catcher observations; the presence of all zonal marker species for both diatoms and radiolarians suggests that the local environment was not especially unusual; and most of the species used for zonation in this study are well-known species that have been employed for decades in Southern Ocean biostratigraphic work.

We thus conclude that the most probable reason for the discrepancy between the biostratigraphic and magnetostratigraphic data from Site 1095 is previous miscalibration of Southern Ocean biostratigraphic events to the GPTS in the late Miocene to basal Pliocene time interval. This interval has long been the most difficult part of the entire Neogene Southern Ocean biostratigraphic zonation to calibrate, due to the presence of hiatuses and low sedimentation rates in many, or most, of the sections used previously, plus the difficulty in synthesizing data from multiple holes in the absence of mcd scales (Gersonde et al., 1990; Barron et al., 1991; Harwood et al., 1992). Although our conclusion is tentative and needs to be confirmed by reexamination of those sections used to make the published calibrations, this result, if true, may help to significantly improve the accuracy of Neogene chronologic scales in the Antarctic region.

In the remaining part of the Pliocene section of Site 1095 (~4.5–1.8 Ma; ~150–25 mcd) biostratigraphic and magnetostratigraphic data are in agreement and indicate a (relatively) low sedimentation rate of ~50 m/m.y.

Pleistocene

The age model for Site 1095 in the Pleistocene suggests continuous sedimentation, albeit at a relatively low rate of ~10 m/m.y. An unconformity was based on seismic stratigraphy, coincident with a prominent

lithostratigraphic boundary (53.54 mcd = 57.5 mbsf in figure F4a of the "Site 1095" chapter in the Leg 178 *Initial Reports* volume; Shipboard Scientific Party, 1999b). During Leg 178, Chron C1r.1n. through C2An.2r. could not be confidently identified and the reversal at ~58.8 mbsf (= 54.8 mcd) was interpreted as the termination of the Olduvai (1.77 Ma). The onset of the Olduvai and all of Chron C2r were considered to be lost in a hiatus at the termination of the Olduvai (see "Magnetostratigraphy" in the "Site 1095" chapter; Shipboard Scientific Party, 1999b). Postcruise magnetostratigraphic interpretation using the undisturbed U-channel samples and the composite depth scale suggests that all polarity events are present, and thus no hiatus (within the resolution of the magnetostratigraphic data) needs be proposed (Acton et al., **Chap. 37,** this volume). Postcruise observation of core photographs (digital images are available from **www-odp.tamu.edu/publications/178_IR/VOLUME/CORES/COR_1095.PDF**) by the first author suggests that there is an erosional contact in Section 178-1095D-7H-2, 75 cm (54.55 mcd), at the bottom of a massive coarse sediment layer. All of the other turbidite layers in this section are parallel to the coring direction (perpendicular to the core liner walls). The irregular contact seen at 75 cm in this section is therefore interpreted as an original sedimentary structure, although it was described as core disturbance in the initial report (see "Lithology" in the "Site 1095" chapter; Shipboard Scientific Party, 1999b). This possible erosional contact in Hole 1095D may be correlated to the seismic unconformity observed at this site. This unconformity is considered to be missing in Hole 1095A between Cores 178-1095A-7H and 8H. However, the presence of all expected magnetostratigraphic events and the absence of any noticeable sedimentation rate change suggest that the time gap of the seismic unconformity (possible hiatus) is small and is probably <200 k.y. (Acton et al., **Chap. 37,** this volume).

Site 1096

The age-depth plot for Site 1096 (Fig. **F7**) is in most respects similar to the age equivalent interval in Site 1095, with higher rates of sedimentation (~180 m/m.y) in the Pliocene, giving way to lower rates (~80 m/m.y) in the Pleistocene. Biostratigraphic and magnetostratigraphic data are in good agreement with each other except for several biostratigraphic events, all with age calibrations between 3.2 and 3.8 Ma, which are scattered over a wide depth interval at Site 1096. We have no explanation for this, although one of the events—the top of the radiolarian *Lampromitra coronata*—is only an informal marker which has not been yet studied for biostratigraphic consistency.

Site 1101

Site 1101 is the shortest of the sections studied here and reached only the mid-Pliocene at the base of the hole (217.7 mbsf). The magnetostratigraphic age model fits the biostratigraphic data reasonably well throughout and suggests a nearly constant rate of sedimentation over the entire 0- to 3.0-Ma time interval. Only one event—the top of the radiolarian *Cycladophora pliocenica*—is noticeably offset from the remainder of the data. This event is usually quite reliable in Antarctic stratigraphy. However, the morphology of this species is similar to several other species in the same genus, and it is possible that the discrepancy is due to a taxonomic misidentification, particularly as the

shipboard preparations were characterized by poor sample breakdown, which tends to obscure taxonomically important morphologic detail (Lazarus, **Chap. 13,** this volume).

SUMMARY

During ODP Leg 178, eight holes were drilled at three sites (1095, 1096, and 1101) on the continental rise and ten holes at four sites (1097, 1100, 1102, and 1103) on the continental shelf, respectively, of the western Antarctic Peninsula (Barker, Camerlenghi, Acton, et al., 1999).

Excellent magnetostratigraphic and generally good biostratigraphic control is present for the past ~9.6 m.y. at Sites 1095, 1096, and 1101 on the sediment drifts. Diatoms and radiolarians offer the best biostratigraphic control for the upper Miocene to middle Pliocene, whereas calcareous nannofossils and planktonic foraminifers are useful in the upper Pliocene to lower Pleistocene section. Leg 178 studies have allowed refinement of the magnetobiochronologic framework for the Cenozoic of the Southern Ocean. Siliceous microfossil stratigraphy from diatoms (Winter and Iwai, **Chap. 29,** this volume; Iwai, 2000a, 2000b) and radiolarians (Weinheimer in Barker, Camerlenghi, Acton, et al., 1999; Lazarus, **Chap. 13,** this volume) provides the basis for much of the stratigraphic division of Leg 178 Neogene sediments presented here (Fig. **F2**). Biostratigraphic control for the early to middle Pleistocene is from calcareous nannofossils (Winter and Wise, **Chap. 26,** this volume; Kameo in Iwai et al., **Chap. 28,** this volume).

The paleomagnetic and biostratigraphic data are mostly in excellent agreement for the three continental rise sites. One exception is that there is a systematic shift of the biostratigraphic events from the depth-age curve derived from magnetostratigraphy in the latest Miocene–earliest Pliocene interval at Site 1095. This shift is not easily explainable in our data by processes such as reworking, downcore contamination, taxonomic confusion, or diachroneity of biostratigraphic events. We suggest that the published magnetobiostratigraphic calibration in the Southern Ocean for the late Miocene–earliest Pleistocene time interval had a problem caused by the unusual common hiatus.

ACKNOWLEDGMENTS

We thank Co-Chief Scientists Peter Barker and Angelo Camerlenghi and all the scientific participants of ODP Leg 178 for their partnership during the cruise, and the crews and shipboard staff for their support. Discussion of sedimentary processes at Site 1095 with Peter Barker, Claus-Dieter Hillenbrand, and Thomas C.W. Wolf-Welling were especially helpful. We also thank Peter Barker and Angelo Camerlenghi for their discussion and suggestion on seismic stratigraphy; Amy L. Weinheimer, Diane Winter, and Koji Kameo for their comments on Biostratigraphy; and Stefanie Brachfeld and Yohan Guyodo for their contribution to the paleomagnetism results. This paper benefitted from careful reviews by A. Ramsey and A. Roberts. This research used samples and/or data provided by the Ocean Drilling Program (ODP). ODP is sponsored by the U.S. National Science Foundation (NSF) and participating countries under management of Joint Oceanographic Institutions (JOI), Inc. Funding for this research was provided by the Ministry

of Education, Culture, Sports, Science, and Technology (MEXT) Grant-in-Aid for scientific research (C) Number 09839042 and Number 13640473, grants from the JOI/United States Science Support Program (USSSP), and DFG ODP Schwerpunktprogramm grants LA 1191/1-1 and 2.

REFERENCES

Baldauf, J.G., and Barron, J.A., 1991. Diatom biostratigraphy: Kerguelen Plateau and Prydz Bay regions of the Southern Ocean. *In* Barron, J., Larsen, B., et al., *Proc. ODP, Sci. Results,* 119: College Station, TX (Ocean Drilling Program), 547–598.

Barker, P.F., and Camerlenghi, A., 1999. An Approach to Antarctic Glacial History: the Aims of Leg 178. *In* Barker, P.F., Camerlenghi, A., Acton, G.D., et al., 1999. *Proc. ODP, Init. Repts.,* 178, 1–44 [CD-ROM]. Available from: Ocean Drilling Program, Texas A&M University, College Station, TX 77845-9547, U.S.A.

Barker, P.F., Camerlenghi, A., Acton, G.D., et al., 1999. *Proc. ODP, Init. Repts.,* 178 [CD-ROM]. Available from: Ocean Drilling Program, Texas A&M University, College Station, TX 77845-9547, U.S.A.

Barron, J.A., Baldauf, J.G., Barrera, E., Caulet, J.-P., Huber, B.T., Keating, B.H., Lazarus, D., Sakai, H., Thierstein, H.R., and Wei, W., 1991. Biochronologic and magnetochronologic synthesis of Leg 119 sediments from the Kerguelen Plateau and Prydz Bay, Antarctica. *In* Barron, J., Larsen, B., et al., *Proc. ODP, Sci. Results,* 119: College Station, TX (Ocean Drilling Program), 813–847.

Berggren, W.A., 1992. Neogene planktonic foraminifer magnetobiostratigraphy of the southern Kerguelen Plateau (Sites 747, 748, and 751). *In* Wise, S.W., Jr., Schlich, R., et al., *Proc. ODP, Sci. Results,* 120 (Pt. 2): College Station, TX (Ocean Drilling Program), 631–647.

Berggren, W.A., Kent, D.V., Flynn, J.J., and van Couvering, J.A., 1985a. Cenozoic geochronology. *Geol. Soc. Am. Bull.,* 96:1407–1418.

Berggren, W.A., Kent, D.V., Swisher, C.C., III, and Aubry, M.-P., 1995. A revised Cenozoic geochronology and chronostratigraphy. *In* Berggren, W.A., Kent, D.V., Aubry, M.-P., and Hardenbol, J. (Eds.), *Geochronology, Time Scales and Global Stratigraphic Correlation.* Spec. Publ.—SEPM (Soc. Sediment. Geol.), 54:129–212.

Berggren, W.A., Kent, D.V., and Van Couvering, J.A., 1985b. The Neogene, Part 2. Neogene geochronology and chronostratigraphy. *In* Snelling, N.J. (Ed.), *The Chronology of the Geological Record.* Geol. Soc. London Mem., 10:211–260.

Bukry, D., 1973. Low-latitude coccolith biostratigraphic zonation. *In* Edgar, N.T., Saunders, J.B., et al., *Init. Repts. DSDP,* 15: Washington (U.S. Govt. Printing Office), 685–703.

————, 1975. Coccolith and silicoflagellate stratigraphy near Antarctica, Deep Sea Drilling Project, Leg 28. *In* Hayes, D.E., Frakes, L.A., et al., *Init. Repts. DSDP,* 28: Washington (U.S. Govt. Printing Office), 709–723.

————, 1978. Biostratigraphy of Cenozoic marine sediment by calcareous nannofossils. *Micropaleontology,* 24:44–60.

Cande, S.C., and Kent, D.V., 1995. Revised calibration of the geomagnetic polarity timescale for the Late Cretaceous and Cenozoic. *J. Geophys. Res.,* 100:6093–6095.

Caulet, J.-P., 1991. Radiolarians from the Kerguelen Plateau, Leg 119. *In* Barron, J., Larsen, B., et al., *Proc. ODP, Sci. Results,* 119: College Station, TX (Ocean Drilling Program), 513–546.

Chen, P.-H., 1975. Antarctic radiolaria. *In* Hayes, D.E., Frakes, L.A., et al., *Init. Repts. DSDP,* 28: Washington (U.S. Govt. Printing Office), 437–513.

Gartner, S., 1977. Calcareous nannofossil biostratigraphy and revised zonation of the Pleistocene. *Mar. Micropaleontol.,* 2:1–25.

————, 1990. Neogene calcareous nannofossil biostratigraphy, Leg 116 (Central Indian Ocean). *In* Cochran, J.R., Stow, D.A.V., et al., *Proc. ODP, Sci. Results,* 116: College Station, TX (Ocean Drilling Program), 165–187.

Gersonde, R., Abelmann, A., Burckle, L.H., Hamilton, N., Lazarus, D., McCartney, K., O'Brien, P., Spiess, V., and Wise, S.W., Jr., 1990. Biostratigraphic synthesis of Neogene siliceous microfossils from the Antarctic Ocean, ODP Leg 113 (Weddell Sea). *In* Barker, P.F., Kennett, J.P., et al., *Proc. ODP, Sci. Results,* 113: College Station, TX (Ocean Drilling Program), 915–936.

Gersonde, R., and Bárcena, M.A., 1998. Revision of the late Pliocene-Pleistocene diatom biostratigraphy for the northern belt of the Southern Ocean. *Micropaleontology,* 44:84–98.

Gersonde, R., and Burckle, L.H., 1990. Neogene diatom biostratigraphy of ODP Leg 113, Weddell Sea (Antarctic Ocean). *In* Barker, P.F., Kennett, J.P., et al., *Proc. ODP, Sci. Results,* 113: College Station, TX (Ocean Drilling Program), 761–789.

Gersonde, R., Hodell, D.A., Blum, P., et al., 1999. *Proc. ODP, Init. Repts.,* 177 [CD-ROM]. Available from: Ocean Drilling Program, Texas A&M University, College Station, TX 77845-9547, U.S.A.

Harwood, D.M., Lazarus, D.B., Abelmann, A., Aubry, M.-P., Berggren, W.A., Heider, F., Inokuchi, H., Maruyama, T., McCartney, K., Wei, W., and Wise, S.W., Jr., 1992. Neogene integrated magnetobiostratigraphy of the central Kerguelen Plateau, Leg 120. *In* Wise, S.W., Jr., Schlich, R., et al., *Proc. ODP, Sci. Results,* 120: College Station, TX (Ocean Drilling Program), 1031–1052.

Harwood, D.M., and Maruyama, T., 1992. Middle Eocene to Pleistocene diatom biostratigraphy of Southern Ocean sediments from the Kerguelen Plateau, Leg 120. *In* Wise, S.W., Jr., Schlich, R., et al., *Proc. ODP, Sci. Results,* 120: College Station, TX (Ocean Drilling Program), 683–733.

Hays, J.D., 1965. Radiolaria and late Tertiary and Quaternary history of Antarctic seas. *In* Llano, G.A. (Ed.), *Biology of the Antarctic Seas II.* Antarct. Res. Ser., 5:125–184.

Hilgen, F.J., 1991a. Astronomical calibration of Gauss to Matuyama sapropels in the Mediterranean and implication for the geomagnetic polarity time scale. *Earth Planet. Sci. Lett.,* 104:226–244.

————, 1991b. Extension of the astronomically calibrated (polarity) time scale to the Miocene/Pliocene boundary. *Earth Planet. Sci. Lett.,* 107:349–368.

Hollister, C.D., Craddock, C., et al., 1976. *Init. Repts. DSDP,* 35: Washington (U.S. Govt. Printing Office).

Iwai, M., 2000a. Diatom age assignment for ODP Leg 178 shelf sites and its implication to the late Neogene ice history based on quantitative analysis at Site 1095 and Site 1097, west Antarctic Peninsula. *Eos, Transactions, Am. Geophys. Union,* 81:F751.

————, 2000b. Paleocanographic implication of late Miocene to Pliocene fossil diatoms from Site 1095, Antarctic Peninsula. *Eos, Transactions, Am Geophys. Union,* 81:S271.

————, 2001. Antarctic shelf paleobathymetry and Polar Front migrations: diatom evidence from ODP Site 1095, Antarctic Peninsula. *Program and abstracts: 7th International Conference on Paleoceanography,* 125 (September 16–22, 2001, Sapporo, Japan).

Jenkins, D.G., and Srinivasan, M.S., 1986. Cenozoic planktonic foraminifers from the equator to the sub-Antarctic of the southwest Pacific. *In* Kennett, J.P., von der Borch, C.C., et al., *Init. Repts. DSDP,* 90: Washington (U.S. Govt. Printing Office), 795–834.

Keany, J., 1979. Early Pliocene radiolarian taxonomy and biostratigraphy in the Antarctic region. *Micropaleontology,* 25:50–74.

Langereis, C.G., Van Hoof, A.M., and Hilgen, F.J., 1994. Steadying the rates. *Nature,* 369:615.

Lazarus, D., 1990. Middle Miocene to Recent radiolarians from the Weddell Sea, Antarctica, ODP Leg 113. *In* Barker, P.F., Kennett, J.P., et al., *Proc. ODP, Sci. Results,* 113: College Station, TX (Ocean Drilling Program), 709–727.

————, 1992. Antarctic Neogene radiolarians from the Kerguelen Plateau, Legs 119 and 120. *In* Wise, S.W., Jr., Schlich, R., et al., *Proc. ODP, Sci. Results,* 120: College Station, TX (Ocean Drilling Program), 785–809.

Martini, E., 1971. Standard Tertiary and Quaternary calcareous nannoplankton zonation. *In* Farinacci, A. (Ed.), *Proc. 2nd Int. Conf. Planktonic Microfossils Roma:* Rome (Ed. Tecnosci.), 2:739–785.

Okada, H., and Bukry, D., 1980. Supplementary modification and introduction of code numbers to the low-latitude coccolith biostratigraphic zonation (Bukry, 1973; 1975). *Mar. Micropaleontol.,* 5:321–325.

Pujos, A., 1988. Spatio-temporal distribution of some Quaternary coccoliths. *Oceanol. Acta,* 11:65–77.

Raffi, I., Backman, J., Rio, D., and Shackleton, N.J., 1993. Plio-Pleistocene nannofossil biostratigraphy and calibration to oxygen isotopes stratigraphies from Deep Sea Drilling Project Site 607 and Ocean Drilling Program Site 677. *Paleoceanography,* 8:387–408.

Raffi, I., and Flores, J.-A., 1995. Pleistocene through Miocene calcareous nannofossils from eastern equatorial Pacific Ocean. *In* Pisias, N.G., Mayer, L.A., Janecek, T.R., Palmer-Julson, A., and van Andel, T.H. (Eds.), *Proc. ODP, Sci. Results,* 138: College Station, TX (Ocean Drilling Program), 233–286.

Ramsay, A.T.S., and Baldauf, J.G., 1999. A reassessment of the Southern Ocean biochronology. *Mem.—Geol. Soc. Am.,* 18:1–122.

Rebesco, M., Camerlenghi, A., and Zanolla, C., 1998. Bathymetry and morphogenesis of the continental margin west of the Antarctic Peninsula. *Terra Antart.,* 5:715–728.

Rebesco, M., Larter, R.D., Barker, P.F., Camerlenghi, A., and Vanneste, L.E., 1997. The history of sedimentation on the continental rise west of the Antarctic Peninsula. *In* Barker, P.F., and Cooper, A.K. (Eds.), *Geology and Seismic Stratigraphy of the Antarctic Margin* (Pt. 2). Am. Geophys. Union, Antarctic Res. Ser., 71:29–50.

Shackleton, N.J., Berger, A., and Peltier, W.A., 1990. An alternative astronomical calibration of the lower Pleistocene timescale based on ODP Site 677. *Trans. R. Soc. Edinburgh: Earth Sci.,* 81:251–261.

Shackleton, N.J., Crowhurst, S., Hagelberg, T., Pisias, N.G., and Schneider, D.A., 1995. A new late Neogene time scale: application to Leg 138 sites. *In* Pisias, N.G., Mayer, L.A., Janecek, T.R., Palmer-Julson, A., and van Andel, T.H. (Eds.), *Proc. ODP, Sci. Results,* 138: College Station, TX (Ocean Drilling Program), 73–101.

Shipboard Scientific Party, 1995. Explanatory notes. *In* Curry, W.B., Shackleton, N.J., Richter, C., et al., *Proc. ODP, Init. Repts.,* 154: College Station, TX (Ocean Drilling Program), 11–38.

————, 1999a. Leg 178 summary. *In* Barker, P.F., Camerlenghi, A., Acton, G.D., et al., *Proc. ODP, Init. Repts.,* 178: College Station, TX (Ocean Drilling Program), 1–58.

————, 1999b. Site 1095. *In* Barker, P.F., Camerlenghi, A., Acton, G.D., et al., *Proc. ODP, Init. Repts.,* 178, 1–173 [CD-ROM]. Available from: Ocean Drilling Program, Texas A&M University, College Station, TX 77845-9547, U.S.A.

————, 1999c. Site 1096. *In* Barker, P.F., Camerlenghi, A., Acton, G.D., et al., *Proc. ODP, Init. Repts.,* 178, 1–144 [CD-ROM]. Available from: Ocean Drilling Program, Texas A&M University, College Station, TX 77845-9547, U.S.A.

————, 1999d. Site 1101. *In* Barker, P.F., Camerlenghi, A., Acton, G.D., et al., *Proc. ODP, Init. Repts.,* 178, 1–83 [CD-ROM]. Available from: Ocean Drilling Program, Texas A&M University, College Station, TX 77845-9547, U.S.A.

Takayama, T., and Sato, T., 1987. Coccolith biostratigraphy of the North Atlantic Ocean, Deep Sea Drilling Project Leg 94. *In* Ruddiman, W.F., Kidd, R.B., Thomas, E., et al., *Init. Repts. DSDP,* 94 (Pt. 2): Washington (U.S. Govt. Printing Office), 651–702.

Thierstein, H.R., Geitzenauer, K.R., and Molfino, B., 1977. Global synchroneity of late Quaternary coccolith datum levels: validation by oxygen isotopes. *Geol. Soc. Am. Bull.,* 5:400–404.

Thomas, E., Barrera, E., Hamilton, N., Huber, B.T., Kennett, J.P., O'Connell, S.B., Pospichal, J.J., Speiss, V., Stott, L.D., Wei, W., and Wise, S.W., Jr., 1990. Upper Cretaceous-Paleogene stratigraphy of Sites 689 and 690, Maud Rise (Antarctica). *In* Barker, P.F., Kennett, J.P., et al., *Proc. ODP, Sci. Results,* 113: College Station, TX (Ocean Drilling Program), 901–914.

Weaver, F.M., 1976. Antarctic Radiolaria from the southeast Pacific basin, Deep Sea Drilling Project, Leg 35. *In* Hollister, C.D., Craddock, C., et al., *Init. Repts. DSDP,* 35: Washington (U.S. Govt. Printing Office), 569–603.

Wei, W., 1993. Calibration of Upper Pliocene-Lower Pleistocene nannofossil events with oxygen isotope stratigraphy. *Paleoceanography,* 8:85–99.

Winter, D.M., and Harwood, D.M., 1997. Integrated diatom biostratigraphy of late Neogene drillholes in Southern Victoria Land and correlation to Southern Ocean records. *In* Ricci, C.A. (Ed.), *The Antarctic Region: Geological Evolution and Processes.* Terra Antart. Publ., 985–992.

Figure F1. Location of ODP Leg 178 sites with shaded bathymetric contours (modified from Rebesco et al., 1998).

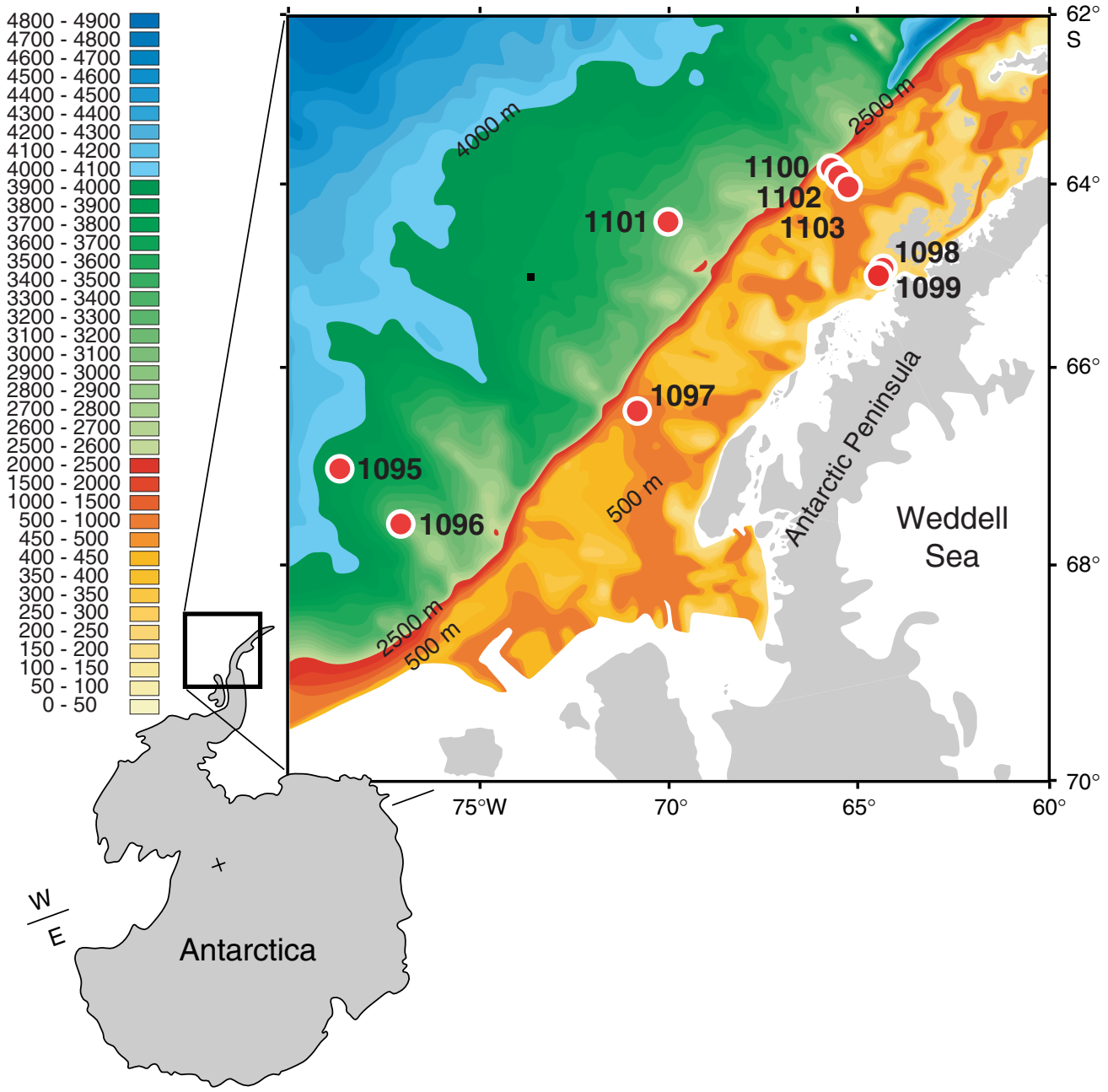

Figure F2. Summary of the Neogene chronostratigraphy adopted for Leg 178 studies. Geomagnetic polarity timescale is after Cande and Kent (1995). Sources for calibration of each zonation: 1 = Berggren et al., 1995, 2 = Cande and Kent, 1995, 3 = Harwood and Maruyama, 1992; Winter and Iwai, Chap. 29, this volume; Iwai, 2001, unpubl. data, 4 = Lazarus, 1992, 5 = Okada and Bukry, 1980, 6 = Martini, 1971, 7 = Berggren, 1992.

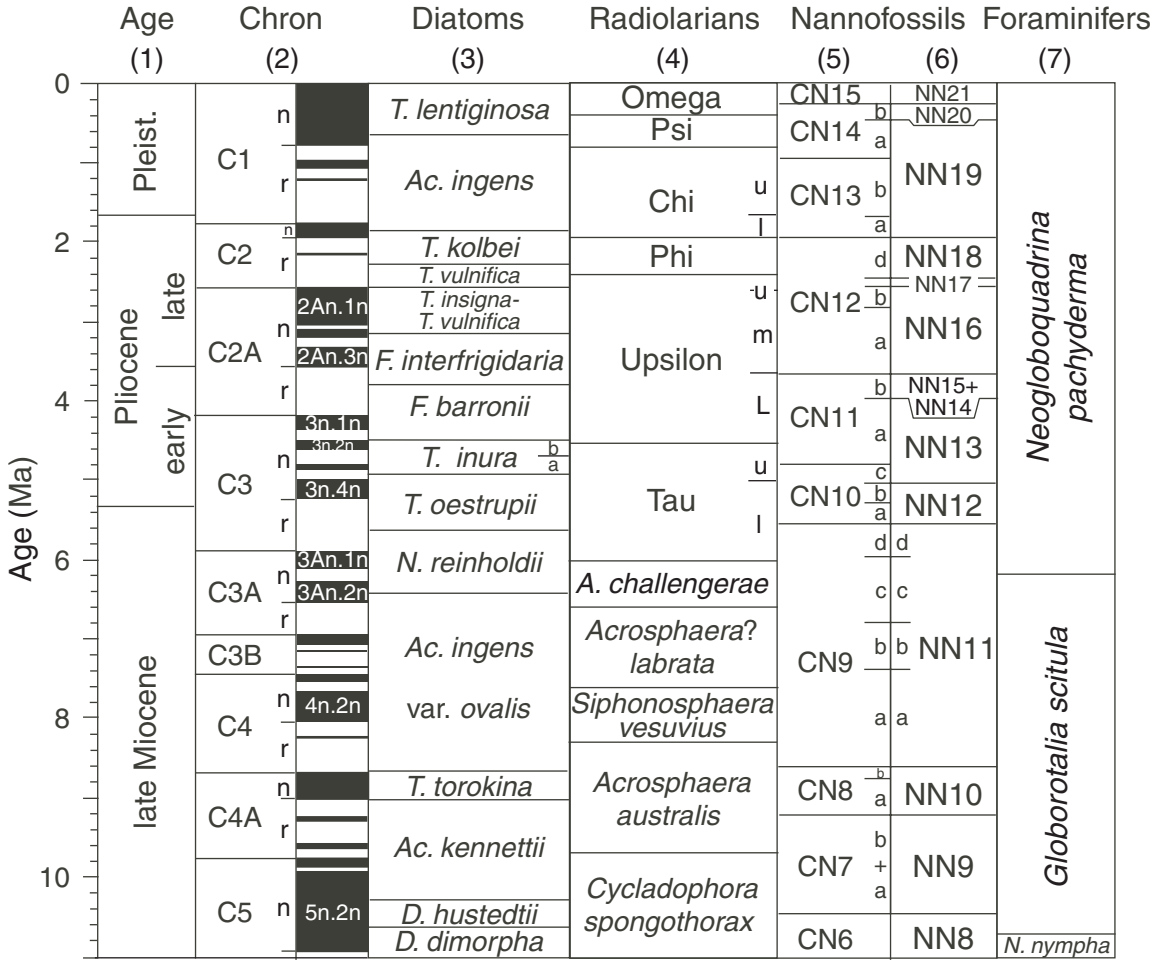

Figure F3. Magnetostratigraphic and biostratigraphic summary of Site 1095. A zonal boundary which was identified to within one core is shown by a horizontal solid line. Dashed lines are used for more tentative event positions. 1 = Acton et al., **Chap. 37,** this volume, 2 = Winter and Iwai, **Chap. 29,** this volume; Iwai, 2000a, 2001, 3 = Lazarus, **Chap. 13,** this volume, 4 = Iwai et al., **Chap. 28,** this volume, 5 = Osterman in Barker, Camerlenghi, Acton, et al., 1999, 6 = Berggren et al., 1995, 7 = wavy lines represent a seismically identified uncomformity (Barker, Camerlenghi, Acton, et al., 1999).

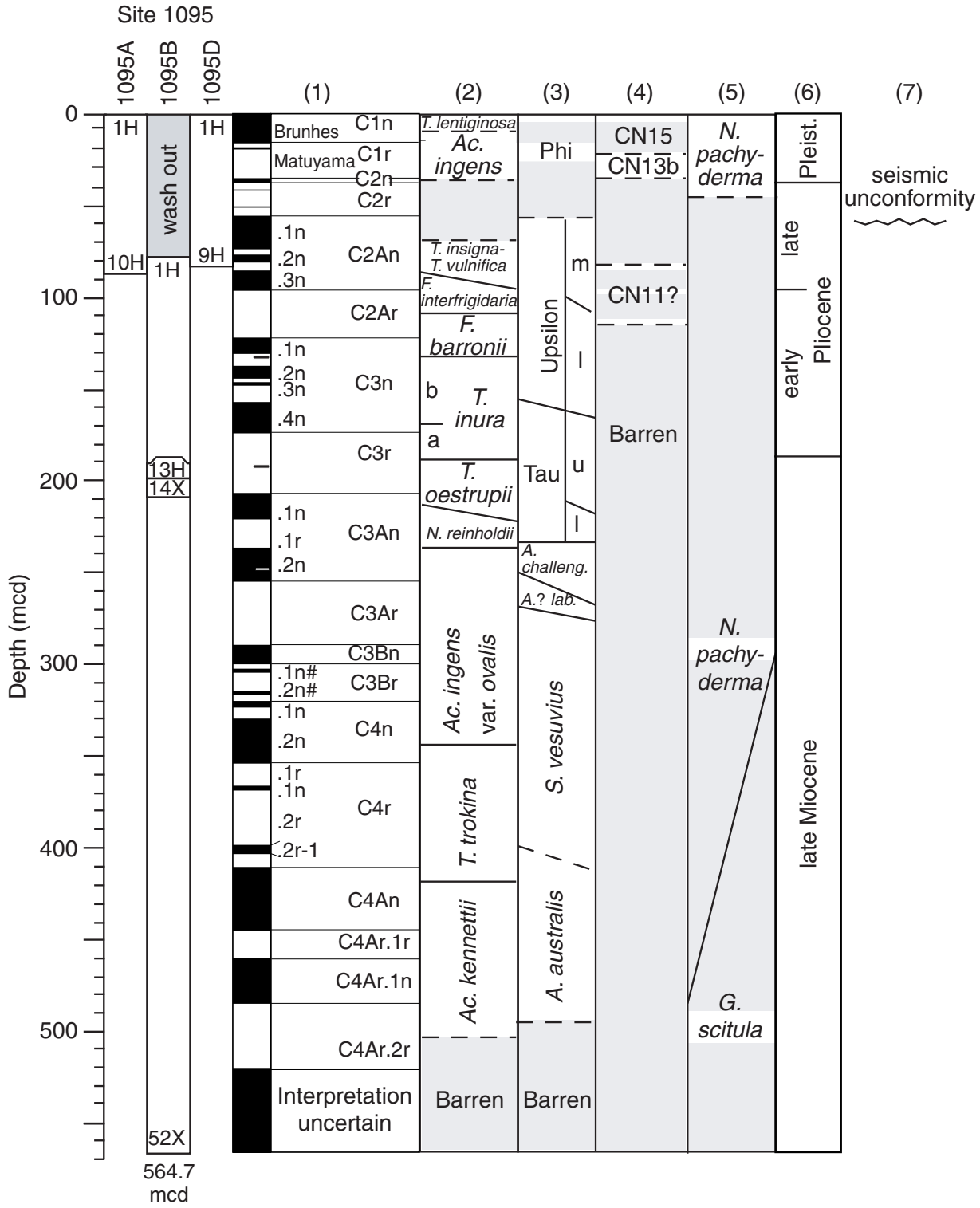

Figure F4. Magnetostratigraphic and biostratigraphic summary of Site 1096. 1 = Acton et al., **Chap. 37,** this volume, 2 = Winter and Iwai, **Chap. 29,** this volume, 3 = Weinheimer in Barker, Camerlenghi, Acton, et al., 1999, 4 = Winter and Wise, **Chap. 26,** this volume, 5 = Osterman in Barker, Camerlenghi, Acton, et al., 1999, 6 = Berggren et al., 1995.

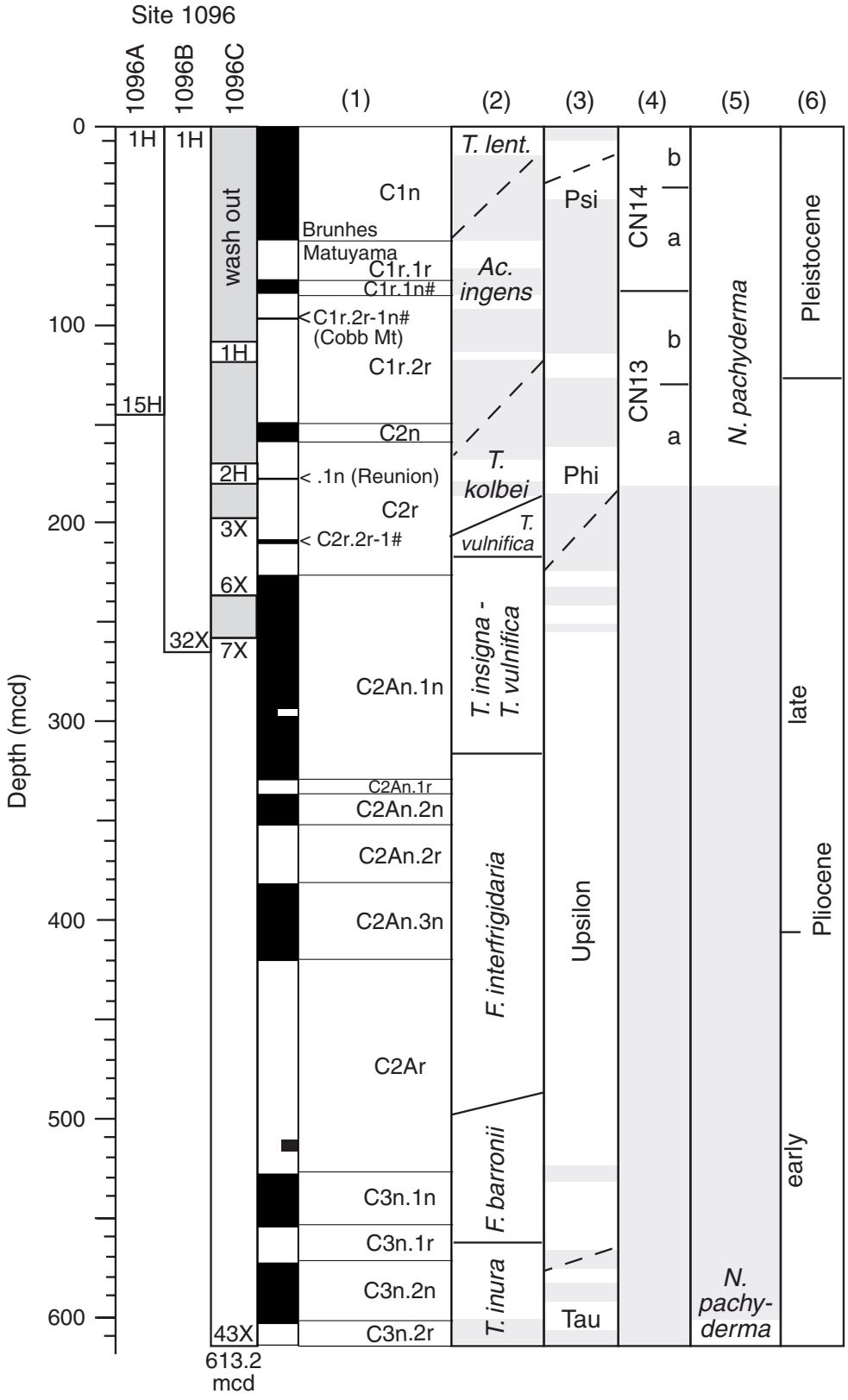

Figure F5. Magnetostratigraphic and biostratigraphic summary of Site 1101. 1 = Acton et al., **Chap. 37,** this volume, 2 = Winter and Iwai, **Chap. 29,** this volume, 3 = Weinheimer in Barker, Camerlenghi, Acton, et al., 1999, 4 = Winter and Wise, **Chap. 26,** this volume, 5 = Osterman in Barker, Camerlenghi, Acton, et al., 1999, 6 = Berggren et al., 1995.

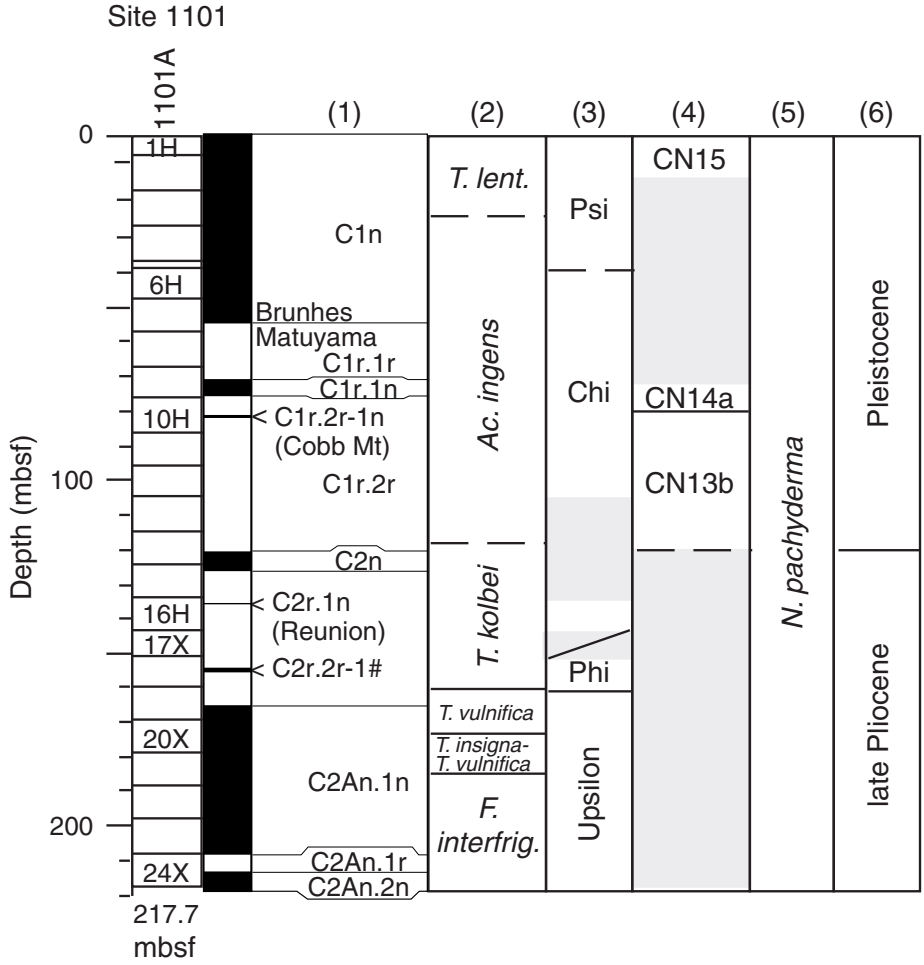

Figure F6. Age-depth profile at Site 1095 with magnetostratigraphic and biostratigraphic events and correlation to the GPTS. Crosses mark magnetostratigraphic events from Table T7, p. 38, as interpreted by Acton et al. (Chap. 37, this volume) and discussed in "Magnetostratigraphic Summary," p. 7, in "Site 1095" in "Data Sources: Magnetobiochronology of Leg 178 Rise Sites." Biostratigraphic events are from Table T4, p. 34. At the plot scale shown, most events are located precisely enough that triangles overlap. D = diatom event code, R = radiolarian event code, N = calcareous nannofossil event code. (t) = top, (b) = bottom. Biostratigraphic event codes are given in Table T2, p. 30. Approximate average sedimentation rates are shown in meters per million years.

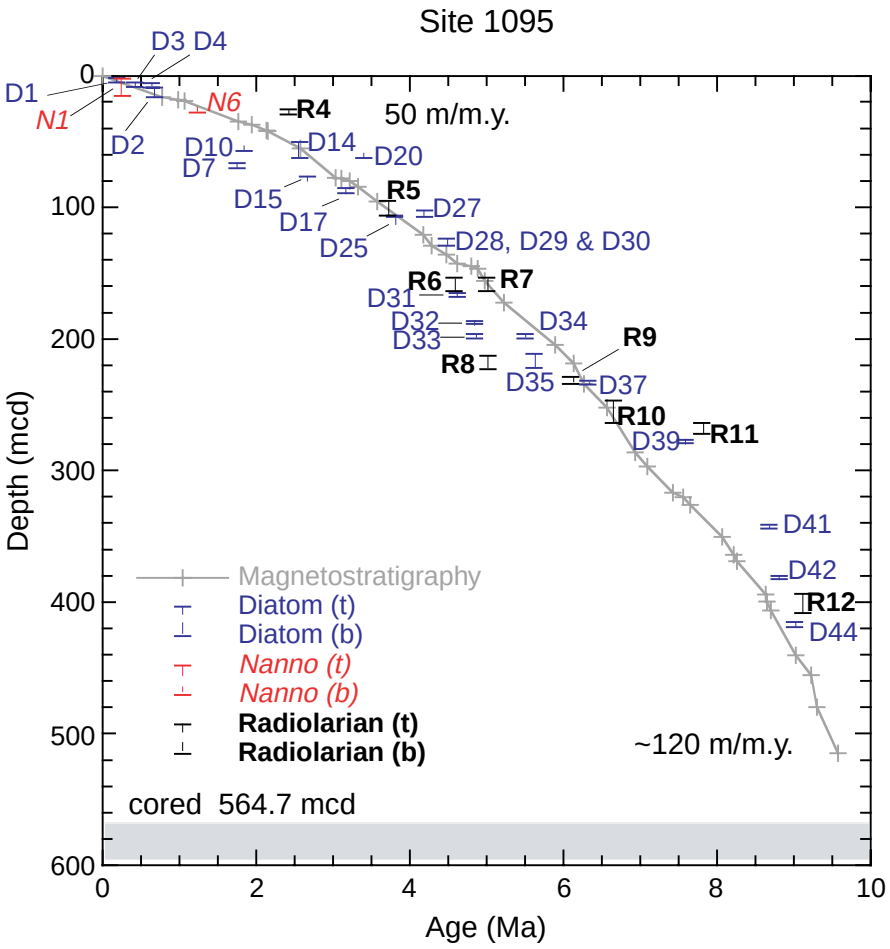

Figure F7. Age-depth profile at Site 1096 with biostratigraphic events. Data are from Tables T5, p. 35, and T7, p. 38. At the plot scale shown, most events are located precisely enough that triangles overlap. D = diatom event code, R = radiolarian event code, N = calcareous nannofossil event code. (t) = top, (b) = bottom. Biostratigraphic event codes are given in Table T2, p. 30. Approximate average sedimentation rates are shown in meters per million years.

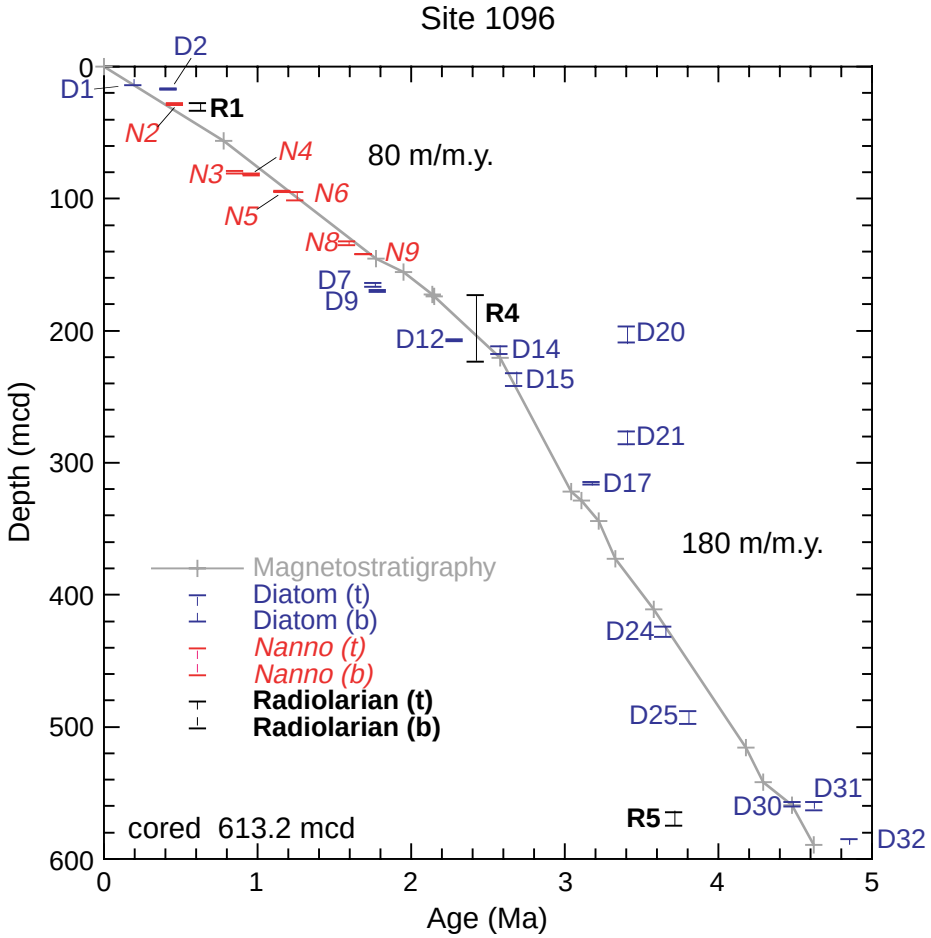

Figure F8. Age vs. depth profile at Site 1101 with biostratigraphic events. Data are from Tables T5, p. 35, and T7, p. 38. At the plot scale shown, most events are located precisely enough that triangles overlap. D = diatom event code, R = radiolarian event code, N = calcareous nannofossil event code. (t) = top, (b) = bottom. Biostratigraphic event codes are given in Table T2, p. 30. Approximate average sedimentation rates are shown in meters per million years.

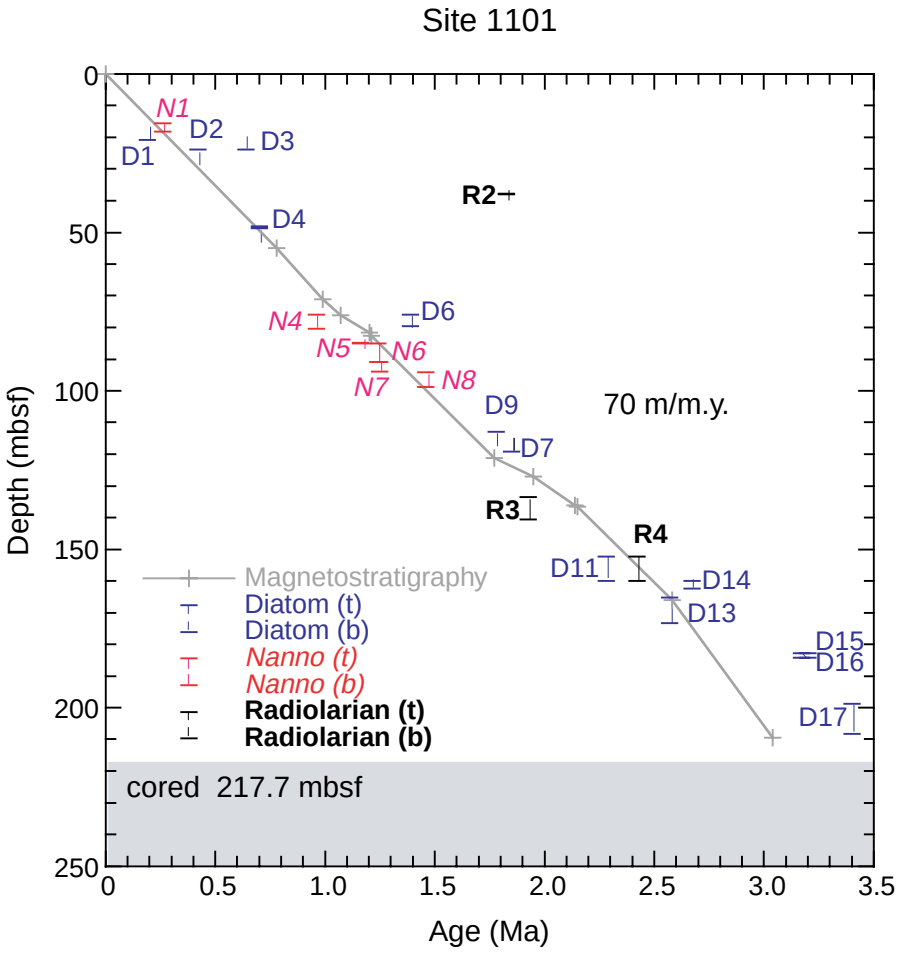

Figure F9. The magnetostratigraphy of Site 1095 based on paleomagnetic inclination data and downhole magnetic logging data. The inclination data are from split-core sections (after 20- to 30-mT demagnetization), U-channel samples (PCA = directions estimated from principal component analysis), and discrete samples (PCA). The magnetic logging data, represented by the remanent anomaly, are from the second pass of the GHMT logging tool in Hole 1095B. The interpreted magnetostratigraphy is also compared with the polarity zonation predicted from the geomagnetic polarity timescale (GPTS) for the case where the sedimentation rates are constant over long periods of time. * = excursions, cryptochrons, or anomalous polarity zones observed in the inclination data, # = chrons and subchrons not identified in the sedimentary section.

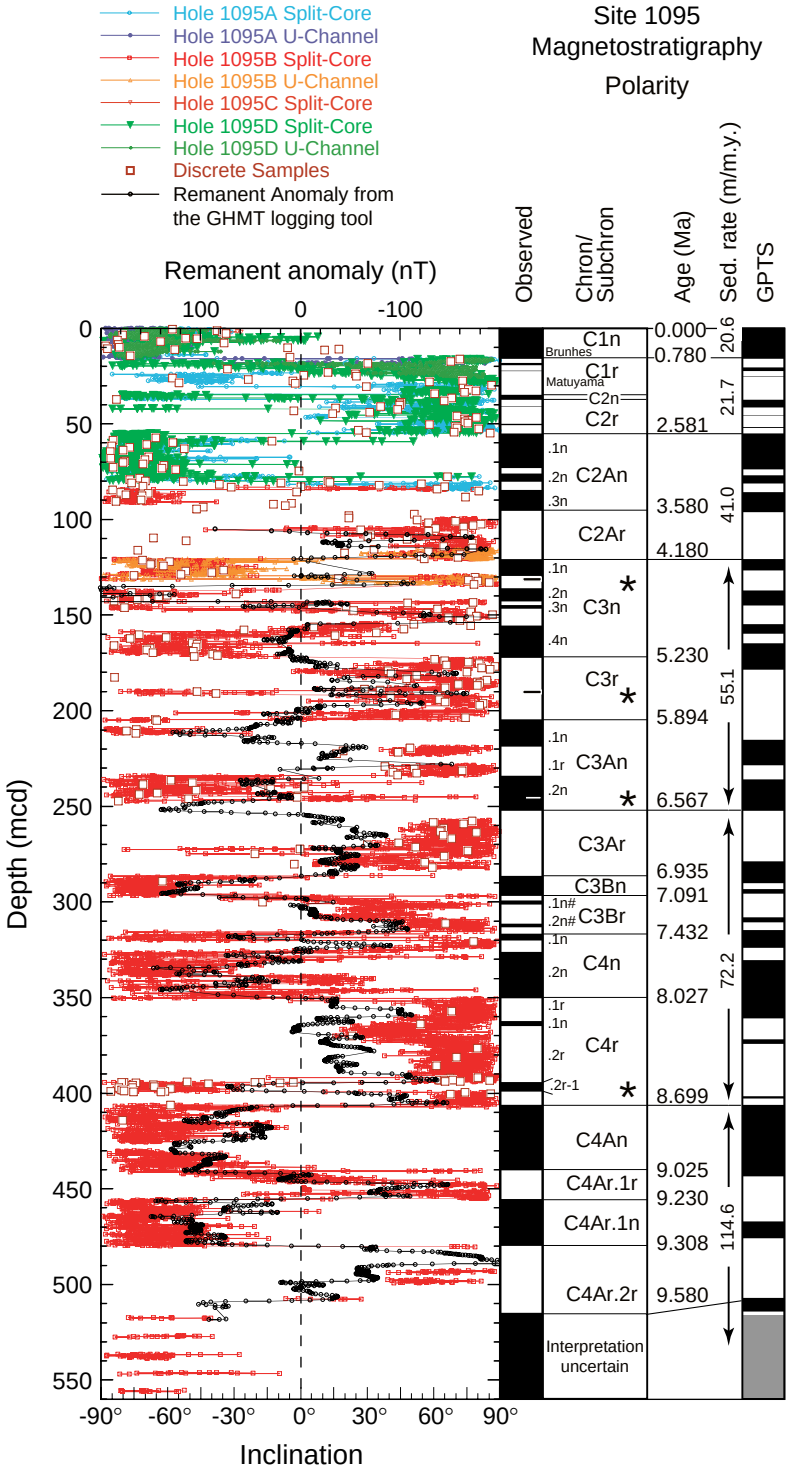

Table T1. Summary of holes cored during Ocean Drilling Program (ODP) Leg 178.

Leg 178	Latitude	Longitude	Water depth (m)	Number of cores	Recovered (%)	Drilled (mbsf)	Drilled (mcd)
1095A	66°59.1′S	78°29.2′W	3841.6	10	99.1	0.00–87.30	0.00–85.76
1095B	66°59.1′S	78°29.3′W	3841.6	52	79.2	83.00–570.20	78.86–564.70
1095C	66°59.1′S	78°29.3′W	3841.6	1	99	0.00–2.90	0.00–2.90
1095D	66°59.1′S	78°29.3′W	3840.9	9	93.3	0.00–84.60	0.00–80.30
1096A	67°34.0′S	76°57.8′W	3152	15	84.2	0.00–140.70	0.24–144.58
1096B	67°34.0′S	76°57.8′W	3152.5	32	80.5	0.00–260.60	0.00–265.92
1096C	67°34.0′S	76°57.8′W	3152.5	43	84.2	114.00–607.70	119.45–613.24
1097A	66°23.6′S	70°45.4′W	551.7	51	13.6	0.00–436.60	
1098A	64°51.7′S	64°12.5′W	1012	7	99.7	0.00–45.90	0.00–49.04
1098B	64°51.7′S	64°12.5′W	1010.6	5	103.9	0.00–43.00	0.06–44.74
1098C	64°51.7′S	64°12.5′W	1010.4	5	99.1	0.00–46.70	0.00–51.09
1099A	64°56.7′S	64°18.9′W	1399.8	7	102.3	0.00–62.30	0.00–62.30
1099B	64°56.7′S	64°18.9′W	1399.8	5	101.8	60.00–107.50	60.00–107.50
1100A	63°53.0′S	65°42.3′W	458.6	4	0	0.00–33.80	
1100B	63°53.0′S	65°42.3′W	458.6	1	7.5	33.90–35.90	
1100C	63°53.0′S	65°42.4′W	458.6	1	81	0.00–5.00	
1101A	64°22.3′S	70°15.7′W	3279.7	24	99.1	0.00–217.70	
1102A	63°48.2′S	65°51.5′W	430.5	1	5.3	0.00–7.90	
1102B	63°48.2′S	65°51.5′W	430.5	1	5.2	0.00–7.50	
1102C	63°48.1′S	65°51.5′W	430.5	2	0.2	0.00–6.50	
1102D	63°48.1′S	65°51.4′W	430.5	1	5.7	0.00–14.90	
1103A	63°60.0′S	65°27.9′W	493.5	38	12.3	0.00–362.70	

Table T2. Published ages of biostratigraphic events used during Leg 178. (**See table notes.** Continued on next page.)

Event	Published age (Ma) references	Age (Ma)	Event code
Diatoms:			
TC *Hemidiscus karstenii*	0.19 (4, 6); 0.195 (2)	0.19	D1
BC *Hemidiscus karstenii*	0.42 (4, 6)	0.42	D2
T *Actinocyclus ingens*	0.64 (3, 5, 6); 0.65 (4)	0.64	D3
T *Thalassiosira elliptipora*	0.68 (3, 6); 0.7 (5)	0.68	D4
T *Fragilariopsis barronii*	1.3 (4); 1.39 (3, 6)	1.39	D5
T *Thalassiosira fasciculata*	0.70 (5); 1.7 (3, 6)	1.7	D6
T *Thalassiosira inura*	1.75 (3, 6); 2.5 (5)	1.75	D7
B *Thalassiosira elliptipora*	1.77? (3, 5, 6)	1.77	D8
T *Actinocyclus karstenii*	1.78-2.9 (3, 6)	1.78	D9
T *Thalassiosira torokina*	1.8 (2, 5); 1.85 (3, 6)	1.85	D10
T *Thalassiosira kolbei*	1.85 (3, 6); 2 (2, 4, 5)	1.85	D11
T *Thalassiosira vulnifica*	2.28 (3, 6); 2.5 (2, 5)	2.28	D12
B *Thalassiosira gracilis*	2.28 (3, 6)	2.28	D13
T *Thalassiosira insigna*	2.57 (3, 6); 2.6 (4); 2.63 (5)	2.57	D14
T *Fragilariopsis interfrigidaria*	2.63 (5); 2.67 (3, 6)	2.67	D15
T *Fragilariopsis weaveri*	2.65 (2, 5); 2.7 (3, 6)	2.7	D16
B *Thalassiosira vulnifica*	3.17 (3, 6); 3.26 (2, 5)	3.17	D17
B *Fragilariopsis kerguerensis*	2.70? (5); 3.33 (3, 6)	3.33	D18
T *Thalassiosira striata*	2.92-3.4 (3, 6)	2.92–3.4	D19
T *Thalassiosira complicata*	2.5 (5); 3.4 (3, 6)	3.4	D20
B *Thalassiosira insigna*	3.4 (2, 3, 5, 6)	3.4	D21
B *Fragilariopsis weaveri*	3.4 (2, 3, 5, 6)	3.4	D22
B *Fragilariopsis ritscherii*	3.53 (3, 6)	3.53	D23
T *Fragilariopsis praeinterfrigidaria*	3.64 (3, 6); 3.8 (1, 2, 5)	3.64	D24
B *Fragilariopsis interfrigidaria*	3.8 (1, 2, 3, 5, 6)	3.8	D25
B *Thalassiosira kolbei*	3.75? (2, 5); 4.07 (3, 6)	4.07	D26
B *Thalassiosira lentignosa*	4.2 (3, 6)	4.2	D27
B *Thalassiosira striata*	4.48 (3, 6)	4.48	D28
B *Thalassiosira fasciculata*	4.48 (3, 6); 4.50 (4, 5)	4.48	D29
B *Fragilariopsis barronii*	4.44 (5); 4.48 (1, 3, 6)	4.48	D30
B *Thalassiosira complicata*	4.44 (5); 4.62 (3, 6)	4.62	D31
B *Thalassiosira inura*	4.85 (3, 6); 4.92 (5)	4.85	D32
B *Fragilariopsis praeinterfrigidaria*	4.85 (3, 6); 5.3 (5)	4.85	D33
B *Thalassiosira tetraoestrupii*	5.49-5.50 (7)	5.50	D34
B *Thalassiosira oestrupii*	5.56 (5); 5.62 (3, 6)	5.62	D35
T *Denticulopsis hustedtii* s.l.	5.3 (5); 6.28 (3, 6)	6.28	D36
T *Actinocyclus ingens* var. *ovalis*	6.27 (5); 6.32 (3, 6)	6.32	D37
B *Thalassiosira oliverana* s.s.	6.42 (3, 5, 6)	6.42	D38
T *Thalassiosira mahoodii*	7.59 (2)	7.59	D39
B *Nitzschia reinholdii*	8.10 (5)	8.10	D40
B *Actinocyclus ingens* var. *ovalis*	8.68 (3, 5, 6)	8.68	D41
B *Thalassiosira mahoodii*	8.61 (2)	8.81	D42
T *Denticulopsis crassa*	—	—	D43
B *Thalassiosira torokina*	9.01 (2, 3, 5)	9.01	D44
T *Denticulopsis dimorpha*	10.63 (3, 6); 10.7 (2, 5)	10.63	D45
Calcareous nannofossils:			
B *Emiliania huxleyi*	0.26 (6)	0.26	N1
T *Pseudoemiliania lacunosa*	0.46 (6)	0.46	N2
T *Reticulofenestra asanoi*	0.85	0.85	N3
R med. *Gephyrocapsa* spp.	0.96 (6)	0.96	N4
B *Reticulofenestra asanoi*	1.16	1.16	N5
T large *Gephyrocapsa* spp.	1.24 (6)	1.24	N6
T *Helicosphaera selli*	1.25	1.25	N7
B large *Gephyrocapsa* spp.	1.58	1.58	N8
B med *Gephyrocapsa* spp.	1.69 (6)	1.69	N9
Radiolarians:			
T *Antarctissa cylindrica*	0.61 (6)	0.61	R1
T *Cycladophora pliocenica*	1.827 (6)	1.83	R2
T *Euceyrtidium calvertense*	1.925 (6)	1.93	R3
T *Helotholus vema*	2.421 (6)	2.42	R4
T *Lampromitra coronata*	3.705 (6)	3.71	R5
B *Helotholus vema*	4.580 (6)	4.58	R6
B *Desmospyris spongiosa*	4.580 (6)	4.58	R7
TC *Lychnocanium grande*	5.018 (6)	5.02	R8
T *Amphymenium challengerae*	6.097 (6)	6.10	R9
B *Amphymenium challengerae*	6.651 (6)	6.65	R10

Table T2 (continued).

Event	Published age (Ma) references	Age (Ma)	Event code
B *Acrosphaera? labrata*	7.797 (6)	7.80	R11
T *Cycladophora spongothorax*	9.117 (6)	9.12	R12

Notes: T = top, B = bottom, TC = top common occurrence, BC = bottom common occurrence. References: 1 = Gersonde and Burckle, 1990, Leg 113 *Scientific Results*; 2 = Baldauf and Barron, 1991, Leg 119 *Scientific Results*; 3 = Harwood and Maruyama, 1992, Leg 120 *Scientific Results*; 4 = Gersonde and Barcena, 1998; 5 = Gersonde, Hodell, Blum et al., 1999, Leg 177 *Initial Reports*; 6 = Barker, Camerlenghi, Acton, et al., 1999, Leg 178 *Initial Reports*, 7 = Boden, 1993.

Table T3. Sample constraints of biostratigraphic events from continental rise Sites 1095, 1096, and 1101. (Continued on next page.)

Event	Code	Hole 1095A	Hole 1095B	Hole 1095D	Hole 1096A	Hole 1096B	Hole 1096C
		178-1095A	178-1095B-	178-1095D-	178-1096A-	178-1096B-	178-1096C-
TC *Hemidiscus karstenii*	D1	—		1H-2, 40/1H-4, 40	2H-2, 1/2H-4, 127	<2H-4,30	
BC *Hemidiscus karstenii*	D2	—		1H-4, 40/1H-CC	2H-6, 80/2H-7, 10	3H-1,140/3H-CC	
T *Actinocyclus ingens*	D3	1H-CC/2H-3, 90		<2H-3, 32	—	—	
T *Thalassiosira elliptipora*	D4	2H-3, 90/3H-6, 94		1H-CC<?	—	—	
T *Fragilariopsis barronii*	D5	—		—	—	—	
T *Thalassiosira fasciculata*	D6	—		—	—	—	
T *Thalassiosira inura*	D7	8H-CC/9H-3,130		—	Bottom of Hole 1096A	20H-2, 49/20H-4, 49	
T *Actinocyclus karstenii*	D9	—		—		20H-5, 100/20H-6, 49	
T *Thalassiosira torokina*	D10	<8H-3, 27-28		< 7H-4, 50		—	Top of Hole 1096C-
T *Thalassiosira kolbei*	D11	—		—		—	—
T *Thalassiosira vulnifica*	D12	—		—		23X-CC/24X-4, 30	3X-7, 4-5/4X-1, 75-76
T *Thalassiosira insigna*	D14	—	Top of Hole 1095B	6H-CC/7H-CC		26X-3, 90/26X-CC	<7X-CC
T *Fragilariopsis interfrigidaria*	D15	9H-CC<	—	—		28X-CC/29X-4, 63	<8X-1, 51-52
B *Thalassiosira vulnifica*	D17	>10H-7, 14.5-15.5	1H-1, 101-103/2H-2, 57-58	—		29X-CC<	13X-1, 10/13X-2, 80
T *Thalassiosira striata*	D19	—	—	—		—	—
T *Thalassiosira complicata*	D20	—	—	< 7H-CC		24X-CC/26X-1,88	—
B *Thalassiosira insigna*	D21	Bottom of Hole1095A	—	Bottom of Hole 1095D		32X-CC<	8X-CC/9X-CC
T *Fragilariopsis praeinterfrigidaria*	D24		—			Bottom of Hole 1096B	24X-CC/25X-2, 19
B *Fragilariopsis interfrigidaria*	D25		3H-CC/4H-1,104				30X-CC/31X-CC
B *Thalassiosira lentignosa*	D27		3H-5, 7-8/ 4H-1, 128-129				—
B *Thalassiosira striata*	D28		5H-6, 90-92/6H-3, 101-103				—
B *Thalassiosira fasciculata*	D29		5H-6, 90-92/6H-3, 101-103				—
B *Fragilariopsis barronii*	D30		5H-6, 90-92/6H-3, 101-103				38X-1,143-145/38X-3, 45
B *Thalassiosira complicata*	D31		10H-2, 60-61/10H-4, 60-61				38X-1, 143-145/38X-5, 138-140
B *Thalassiosira inura*	D32		12H-4, 41-42/12H-5, 30-31				41X-1, 73-74<
B *Fragilariopsis praeinterfrigidaria*	D33		13H-4, 120-121/14X-1, 9-10				Bottom of Hole 1096C
B *Thalassiosira tetraoestrupii*	D34		13H-4, 120-121/14X-1, 9-10				
B *Thalassiosira oestrupii*	D35		15X-2, 59-61/16X-3, 35-36				
T *Actinocyclus ingens* var. *ovalis*	D37		17X-3, 65-68/17X-5, 31-33				
T *Thalassiosira mahoodii*	D39		22X-1, 92-94/22X-2, 42-44				
B *Actinocyclus ingens* var. *ovalis*	D41		28X-5,104/28X-CC				
B *Thalassiosira mahoodii*	D42		32X-5, 113-115/33X-1, 43-44				
T *Denticulopsis crassa*	D43		35X-1, 100-101/35X-5, 117-119				
B *Thalassiosira torokina*	D44		36X-4, 8-10/36X-6, 118-120				
			Bottom of Hole 1095B				
B *Emiliania huxleyi*	N1	1H-2, 70/3H-5, 18.5		—	—	—	
T *Pseudoemiliania lacunosa*	N2	—		—	3H-C/4H-2, 40	—	
T *Reticulofenestra asanoi*	N3	—		—	—	9H-5, 46/ 9H-6, 61	
R med. *Gephyrocapsa* spp.	N4	—		—	—	9H-6, 61/ 9H-7, 42	
B *Reticulofenestra asanoi*	N5	—		—	—	11H-1, 110/11H-2, 70	
T large *Gephyrocapsa* spp.	N6	4H-6, 14/5H-1, 90		—	—	11H-2, 70/11H-6, 62	
T *Helicosphaera selli*	N7	—		—	—	—	
B large *Gephyrocapsa* spp.	N8	—		—	14H-5, 114/14H-CC	—	
B med *Gephyrocapsa* spp.	N9	—		—	15H-5, 117/15H-CC	—	
T *Antarctissa cylindrica*	R1	—		—	3H-CC/4H-CC	—	

Note: The interval in which the first/last occurrence was observed and the actual depth (mbsf) shown for all three holes. Datums occur in the cores within the interval listed for each species. T = top/last occurrence datum, B = base/first occurrence datum, BC = base common/first common occurrence datum, TC = top common/last occurrence datum. CK95 = Cande and Kent (1995). Shaded boxes = either an interval drilled but not cored or an interval not drilled.

Table T3 (continued).

Event	Code	Hole 1101A
		178-1101A-
TC *Hemidiscus karstenii*	D1	<3H-2,110
BC *Hemidiscus karstenii*	D2	3H-4, 110 <
T *Actinocyclus ingens*	D3	<3H-4, 110
T *Thalassiosira elliptipora*	D4	—
T *Fragilariopsis barronii*	D5	9H-CC/10H-3,30
T *Thalassiosira fasciculata*	D6	6H-CC/7H-1, 75
T *Thalassiosira inura*	D7	—
T *Actinocyclus karstenii*	D9	<13H-6, 68
T *Thalassiosira torokina*	D10	<14H-4, 44
T *Thalassiosira kolbei*	D11	—
T *Thalassiosira vulnifica*	D12	17X-CC/18X-CC
T *Thalassiosira insigna*	D14	19X-3, 70/20X-3,70
T *Fragilariopsis interfrigidaria*	D15	18X-CC/19X-2, 70
B *Thalassiosira vulnifica*	D17	21X-3, 58/21X-4,40
T *Thalassiosira striata*	D19	21X-3, 58/21X-4,40
T *Thalassiosira complicata*	D20	—
B *Thalassiosira insigna*	D21	23X-1, 29/23X-CC
T *Fragilariopsis praeinterfrigidaria*	D24	Bottom of Hole 1101A
B *Fragilariopsis interfrigidaria*	D25	
B *Thalassiosira lentignosa*	D27	
B *Thalassiosira striata*	D28	
B *Thalassiosira fasciculata*	D29	
B *Fragilariopsis barronii*	D30	
B *Thalassiosira complicata*	D31	
B *Thalassiosira inura*	D32	
B *Fragilariopsis praeinterfrigidaria*	D33	
B *Thalassiosira tetraoestrupii*	D34	
B *Thalassiosira oestrupii*	D35	
T *Actinocyclus ingens* var. *ovalis*	D37	
T *Thalassiosira mahoodii*	D39	
B *Actinocyclus ingens* var. *ovalis*	D41	
B *Thalassiosira mahoodii*	D42	
T *Denticulopsis crassa*	D43	
B *Thalassiosira torokina*	D44	
B *Emiliania huxleyi*	N1	2H-5, 90/2H-CC
T *Pseudoemiliania lacunosa*	N2	—
T *Reticulofenestra asanoi*	N3	—
R med. *Gephyrocapsa* spp.	N4	9H-CC/10H-3, 118
B *Reticulofenestra asanoi*	N5	10H-6, 107/10H-CC
T large *Gephyrocapsa* spp.	N6	10H-CC/11H-4, 70
T *Helicosphaera selli*	N7	11H-4, 70/11H-6, 67
B large *Gephyrocapsa* spp.	N8	11H-CC/12H-3, 63
B med *Gephyrocapsa* spp.	N9	—
T *Antarctissa cylindrica*	R1	—

Table T4. Depths of biostratigraphic events, Site 1095.

Event	Code	Hole 1095A depth (upper-lower)		Hole 1095B depth (upper-lower)		Hole 1095D depth (upper-lower)		Site 1095 summary
		(mbsf)	(mcd)	(mbsf)	(mcd)	(mbsf)	(mcd)	(mcd)
TC *Hemidiscus karstenii*	D1	—	—			1.90-4.90	1.90-4.90	1.90-4.90
BC *Hemidiscus karstenii*	D2	—	—			4.90-8.47	4.90-8.47	4.90-8.47
T *Actinocyclus ingens*	D3	5.67-9.80	5.67-8.74			11.92†	8.82	5.67-8.74
T *Thalassiosira elliptipora*	D4	9.80-17.72	8.74-16.52			8.47*	8.47*	8.74-16.52
T *Fragilariopsis barronii*	D5	—	—			—	—	—
T *Thalassiosira fasciculata*	D6	—	—			—	—	—
T *Thalassiosira inura*	D7	68.90-72.60	66.48-70.18			—	—	66.48-70.18
T *Actinocyclus karstenii*	D9	—	—			—	—	—
T *Thalassiosira torokina*	D10	62.07†	58.11†			61.1†	57.3†	57.3†
T *Thalassiosira kolbei*	D11	—	—			—	—	—
T *Thalassiosira vulnifica*	D12	—	—			—	—	—
T *Thalassiosira insigna*	D14	—	—			55.27-65.90	50.51-62.48	50.51-62.48
T *Fragilariopsis interfrigidaria*	D15	78.07*	76.53*	—		—	—	76.53*
T *Thalassiosira vulnifica*	D17	86.94*	85.40*	84.01-94.57	79.57-94.57	—	—	85.4-89.07
T *Thalassiosira striata*	D19	—	—	—	—	—	—	—
T *Thalassiosira complicata*	D20	—	—	—	—	65.9†	62.48†	62.48†
B *Thalassiosira insigna*	D21			—	—			—
T *Fragilariopsis praeinterfrigidaria*	D24							—
B *Fragilariopsis interfrigidaria*	D25			112.07-112.54	106.57-107.04			106.57-107.04
B *Thalassiosira lentignosa*	D27			108.07-112.78	102.57-107.28			102.57-107.28
B *Thalassiosira striata*	D28			129.40-134.51	123.9-129.01			123.90-129.01
B *Thalassiosira fasciculata*	D29			129.40-134.51	123.9-129.01			123.90-129.01
B *Fragilariopsis barronii*	D30			129.40-134.51	123.9-129.01			123.90-129.01
B *Thalassiosira complicata*	D31			170.60-173.60	165.1-168.1			165.10-168.10
B *Thalassiosira inura*	D32			192.41-193.80	186.91-188.3			186.91-188.30
B *Fragilariopsis praeinterfrigidaria*	D33			201.62-205.09	196.12-199.59			196.12-199.59
B *Thalassiosira tetraoestrupii*	D34			201.62-205.09	196.12-199.59			196.12-199.59
B *Thalassiosira oestrupii*	D35			216.79-227.65	211.29-222.15			211.29-222.15
T *Actinocyclus ingens* var. *ovalis*	D37			237.55-240.21	232.05-234.71			232.05-234.71
T *Thalassiosira mahoodii*	D39			283.02-284.02	277.52-278.52			277.52-278.52
B *Actinocyclus ingens* var. *ovalis*	D41			346.84-349.50	341.34-344			341.34-344.00
B *Thalassiosira mahoodii*	D42			385.53-388.13	380.03-382.63			380.03-382.63
T *Denticulopsis crassa*	D43			407.60-413.77	402.10-408.27			402.10-408.27
B *Thalassiosira torokina*	D44			420.78-424.88	415.28-419.38			415.28-419.38
B *Emiliania huxleyi*	N1	2.16-16.64	2.16-16.64			—		2.16-15.44
T *Pseudoemiliania lacunosa*	N2	—	—			—		—
T *Reticulofenestra asanoi*	N3	—	—			—		—
R med. *Gephyrocapsa* spp.	N4	—	—			—		—
B *Reticulofenestra asanoi*	N5	—	—			—		—
T large *Gephyrocapsa* spp.	N6	27.94-31.25	28.04-27.79			—		27.79†
T *Helicosphaera selli*	N7	—	—			—		—
B large *Gephyrocapsa* spp.	N8	—	—			—		—
B med *Gephyrocapsa* spp.	N9	—	—			—		—
T *Antarctissa cylindrica*	R1	—	—			—		—
T *Cycladophora pliocenica*	R2	—	—			—		—
T *Euceyrtidium calvertense*	R3	—	—			—		—
T *Helotholus vema*	R4	—	—			27.51-33.02	25.59-29.32	25.59-29.32
T *Lampromitra coronata*	R5			100.78-112.07	95.28-106.57			95.28-106.57
B *Helotholus vema*	R6			158.83-168.92	153.33-163.42			153.33-163.42
B *Desmospyris spongiosa*	R7			158.83-168.92	153.33-163.42			153.33-163.42
TC *Lychnocanium grande*	R8			218.45-228.76	212.95-223.26			212.95-223.26
T *Amphymenium challengerae*	R9			234.29-239.56	228.79-234.06			228.79-234.06
B *Amphymenium challengerae*	R10			252.58-269.49	247.08-263.99			247.08-263.99
B *Acrosphaera? labrata*	R11			269.49-277.61	263.99-272.11			263.99-272.11
T *Cycladophora spongothorax*	R12			399.37-413.55	393.87-408.05			393.87-408.05

Note: The interval in which the first/last occurrence was observed and the actual depth (mbsf) shown for all three holes. Datums occur in the cores within the interval listed for each species. T = top/last occurrence datum, B = base/first occurrence datum, BC = base common/first common occurrence datum, TC = top common/last common occurrence datum. * = upper, † = lower. CK95 = Cande and Kent (1995). Shaded boxes = either an interval drilled but not cored, or an interval not drilled.

Table T5. Depths of biostratigraphic events at Sites 1096 and 1101. (See table notes. Continued on next page.)

Event	Code	Hole 1096A depth (upper-lower)		Hole 1096B depth (upper-lower)		Hole 1096C depth (upper-lower)		Site 1096 Summary	Hole 1101A depth (upper-lower)
		(mbsf)	(mcd)	(mbsf)	(mcd)	(mbsf)	(mcd)	(mcd)	(mbsf)
TC *Hemidiscus karstenii*	D1	9.36-13.47	10.10-14.21	8.60†	8.72†			14.21†	20.80†
BC *Hemidiscus karstenii*	D2	16.00-16.80	16.74-17.54	14.70-23.05	16.58-23.43			16.74-17.54	23.80*
T *Actinocyclus ingens*	D3	—	—	—	—			—	23.80†
T *Thalassiosira elliptipora*	D4	—	—	—	—			—	—
T *Fragilariopsis barronii*	D5	—	—	—	—			—	76.07-79.50
T *Thalassiosira fasciculata*	D6	—	—	—	—			—	48.23-48.60
T *Thalassiosira inura*	D7			159.69-162.69	163.95-166.95			163.95-166-95	—
T *Actinocyclus karstenii*	D9			164.70-166.62	168.96-170.88			168.96-170.88	112.88†
T *Thalassiosira torokina*	D10			—	—			—	119.14†
T *Thalassiosira kolbei*	D11			—	—	—	—	—	—
T *Thalassiosira vulnifica*	D12			180.97-188.31	186.09-192.43	202.00-203.40	206.64-208.04	206.64-208.04	152.35-160.07
T *Thalassiosira insigna*	D14			206.80-212.38	212.12-217.70	262.26†	267.80†	212.12-217.70	165.30-173.40
T *Fragilariopsis interfrigidaria*	D15			226.94-236.83	232.26-242.15	261.40†	266.94†	232.26-242.15	160.07-162.30
B *Thalassiosira vulnifica*	D17			239.72*	245.04*	308.90-311.10	314.44-316.64	314.44-316.64	182.88-184.20
T *Thalassiosira striata*	D19			—	—	—	—	—	182.88-184.20
T *Thalassiosira complicata*	D20			192.98-203.78	197.10-209.10	—	—	197.10-209.10	—
B *Thalassiosira insigna*	D21			257.21*	262.53*	270.68-280.37	276.22-285.91	276.22-285.91	198.79-208.18
T *Fragilariopsis praeinterfrigidaria*	D24					418.70-426.50	424.24-432.04	424.24-432.04	
B *Fragilariopsis interfrigidaria*	D25					482.75-492.33	488.29-497.87	488.29-497.87	
B *Thalassiosira lentignosa*	D27					—	—	—	
B *Thalassiosira striata*	D28					—	—	—	
B *Thalassiosira fasciculata*	D29					—	—	—	
B *Fragilariopsis barronii*	D30					551.50-555.00	557.04-560.54	557.04-560.54	
B *Thalassiosira complicata*	D31					551.50-557.00	557.04-563.04	557.04-563.04	
B *Thalassiosira inura*	D32					579.80*	585.34*	585.34*	
B *Fragilariopsis praeinterfrigidaria*	D33								
B *Thalassiosira tetraoestrupii*	D34								
B *Thalassiosira oestrupii*	D35								
T *Actinocyclus ingens* var. *ovalis*	D37								
T *Thalassiosira mahoodii*	D39								
B *Actinocyclus ingens* var. *ovalis*	D41								
B *Thalassiosira mahoodii*	D42								
T *Denticulopsis crassa*	D43								
B *Thalassiosira torokina*	D44								
B *Emiliania huxleyi*	N1	—	—	—	—			—	15.60-18.20
T *Pseudoemiliania lacunosa*	N2	25.23-28.60	27.49-29.19	—	—			27.49-29.19	—
T *Reticulofenestra asanoi*	N3	—	—	76.76-78.41	79.37-81.02			79.37-81.02	—
R med. *Gephyrocapsa* spp.	N4	—	—	78.41-79.72	81.02-82.33			81.02-82.33	76.01-80.38
B *Reticulofenestra asanoi*	N5	—	—	90.40-91.50	94.25-95.35			94.25-95.35	84.77-84.94
T large *Gephyrocapsa* spp.	N6	—	—	91.50-97.42	95.35-101.27			95.35-101.27	84.94-90.90
T *Helicosphaera selli*	N7	—	—	—	—			—	90.90-93.87
B large *Gephyrocapsa* spp.	N8	128.84-131.49	132.42-135.37	—	—			132.42-135.37	94.19-98.88
B med *Gephyrocapsa* spp.	N9	138.37-138.45	142.25-142.33	—	—			142.25-142.33	—
T *Antarctissa cylindrica*	R1	25.23-32.89	27.49-33.48	—	—			27.49-33.48	—
T *Cycladophora pliocenica*	R2	—	—	—	—			—	37.98-37.82
T *Euceyrtidium calvertense*	R3	—	—	—	—			—	133.43-140.71
T *Helotholus vema*	R4			168.84-218.06	173.10-223.38	559.37-569.40	—	173.10-223.38	152.35-160.07
T *Lampromitra coronata*	R5						564.91-574.94	564.91-574.94	

Table T5 (continued).

Event	Code	Hole 1096A depth (upper-lower)		Hole 1096B depth (upper-lower)		Hole 1096C depth (upper-lower)		Site 1096 Summary	Hole 1101A depth (upper-lower)
		(mbsf)	(mcd)	(mbsf)	(mcd)	(mbsf)	(mcd)	(mcd)	(mbsf)
B *Helotholus vema*	R6						—	—	
B *Desmospyris spongiosa*	R7								
TC *Lychnocanium grande*	R8								
T *Amphymenium challengerae*	R9								
B *Amphymenium challengerae*	R10								
B *Acrosphaera? labrata*	R11								
T *Cycladophora spongothorax*	R12								

Notes: The interval in which the first/last occurrence was observed and the actual depth (mbsf) shown for all three holes. Datums occur in the cores within the interval listed for each species. T = top/last occurrence datum, B = base/first occurrence datum, BC = base common/first common occurrence datum, TC = top common/last common occurrence datum. * = upper, † = lower. CK95 = Cande and Kent (1995). Shaded boxes = either an interval drilled but not cored, or an interval not drilled.

Table T6. Previous magnetostratigraphic interpretations for Site 1095.

Shipboard observation		Shipboard interpretation*		Hiatus case†		Low sedimentation case	
Split core depth (mbsf)	Logging depth (mbsf)	Event	Age (Ma)	Event	Age (Ma)	Event	Age (Ma)
1095A and 1095B	1095B						
0.00	—	Mud line	0	Mud line	0		
17.12	—	C1n (o)	0.78	C1n (o)	0.78		
23.20	—	C1r.1n (t)	0.99	C1r.1n (t)	0.99		
29.75	—	C1r.1n (o)	1.07	C1r.1n (o)	1.07		
				Possible hiatus			
58.8							
1095D: 58.35	—			Cores 178-1095A-7H and 8H and Section 178-1095D-7H-2, 75 cm	1.25-2.53‡		
60.39	—	C2n (t)	1.77	C2An.1n (t)	2.581		
50-65	—	Possible hiatus		—	—		
83.41	—	C2An.1n (o)	3.04	C2An.1n (o)	3.04		
100.99	—	C2An.3n (o)	3.58	C2An.3n (o)	3.58		
126.20	126.12	C3n.1n (t)	4.18	C3n.1n (t)	4.18		
134.97	137.25	C3n.1n (o)	4.29	C3n.1n (o)	4.29		
141.02	139.84	C3n.2n (t)	4.48	C3n.2n (t)	4.48		
148.49	147.53	C3n.2n (o)	4.62	C3n.2n (o)	4.62		
—	150.35	C3n.3n (t)	4.80	—	—		
—	153.71	C3n.3n (o)	4.89	—	—		
164.49	160.00	C3n.4n (t)	4.98	C3n.3n (t)	4.80	C3n.3n (t)	4.80
177.86	177.78	C3n.4n (o)	5.23	C3n.3n (o)	4.89	C3n.3n (o)	4.89
209.74	205.14	C3An.1n (t)	5.894	C3n.4n (t)	4.98	C3n.4n (t)	4.98
220.99	222.29	C3An.1n (o)	6.137	—	—	C3n.4n (o)	5.23
224.3 (214.7-224.3)	227.3 (227.3-228.5)			Possible hiatus between Cores 178-1095B-15X and 16X	5.04 -6.14**	—	—
239.46	236.91	C3An.2n (t)	6.269	C3An.2n (t)	6.269	C3An.1n (t)	5.894
257.80	260.16	C3An.2n (o)	6.567	C3An.2n (o)	6.567	C3An.2n (o)	6.567
292.04	293.91	C3Bn (t)	6.935	C3Bn (t)	6.935		
304.03	302.75	C3Bn (o)	7.091	C3Bn (o)	7.091		
—	305.04	C3Br.1n (t)	7.135	C3Br.1n (t)	7.135		
—	306.26	C3Br.1n (o)	7.17	C3Br.1n (o)	7.17		
322.23	323.33	C4n.1n (t)	7.432	C4n.1n (t)	7.432		
325.80	325.31	C4n.1n (o)	7.562	C4n.1n (o)	7.562		
331.61	332.16	C4n.2n (t)	7.65	C4n.2n (t)	7.65		
355.67	356.78	C4n.2n (o)	8.072	C4n.2n (o)	8.072		
399.86	403.03	C4r.2r-1 (t)	8.635	C4r.2r-1 (t)	8.635		
404.79	406.08	C4r.2r-1 (o)	8.651	C4r.2r-1 (o)	8.651		
411.72	413.84	C4An (t)	8.699	C4An (t)	8.699		
446.00	447.69	C4An (o)	9.025	C4An (o)	9.025		
460.56	460.94	C4Ar.1n (t)	9.23	C4Ar.1n (t)	9.23		
—	487.00	C4Ar.1n (o)	9.308	C4Ar.1n (o)	9.308		
—	522.82	C4Ar.2n (t)	9.58	C4Ar.2n (t)	9.58		

Notes: * = Barker, Camerlenghi, Acton, et al., 1999; Leg 178 *Initial Reports*. † = Iwai, 2000a, 2000b, unpublished data. (o) = onset, (t) = termination. ‡ = hiatus age was extrapolated using nearest control points. ** = hiatus ages were extrapolated using nearest control points of logging data. Numbers in parenthesis indicate the error range of the depth where the possible hiatus occurred in Hole 1095B.

Table T7. Summary of magnetostratigraphy at Sites 1095, 1096, and 1101. (**See table notes.** Continued on next page.)

Event	Age (Ma)	Hole 1095A (mbsf)	Sample type	Hole 1095B (mbsf)	Sample type	Hole 1095D (mbsf)	Sample type	Summary (mcd)	Hole 1096A (mbsf)	Sample type	Hole 1096B (mbsf)	Sample type	Hole 1096C (mbsf)	Sample type	Summary (mcd)	Hole 1101A (mbsf)	Sample type
Mudline	0	0.00				0.00		0.00			0.00				0.00	0.00	
C1n (o)	0.78	17.24	U			18.09	U	16.04	55.03	U	54.99	U			56.10	55.05	U
C1r.1n (t)	0.99	19.25	U			20.09	U	18.16	—		—				—	71.15	U
C1r.1n (o)	1.07	19.62	U			21.26	U	19.21	—		—				—	76.12	U
C1r.2r-1n (t)	1.201	—				—		—	—		—				—	81.61	U
C1r.2r-1n (t)	1.211	—				—		—	—		—				—	82.53	U
C2n (t)	1.77	38.14	S			40.09	S	34.68			141.25	S			145.51	121.25	U
C2n (o)	1.95	41.29	S			42.14	S	37.33			151.24	S			155.50	126.96	U
C2r.1n (t)	2.14	—				46.60	S	41.84			—		168.23	S	172.87	136.20	S
C2r.1n (o)	2.15	—				47.12	S	42.36			—		169.28	S	173.92	136.63	S
C2An.1n (t)	2.581	—				58.88	S	55.08			215.38	S	215.83	S	220.63	165.98	S
C2An.1n (o)	3.04	79.29	S			81.96	S	77.66					316.46	S	322.00	209.38	S
C2An.2n (t)	3.11	79.52	S			82.22	S	77.95					323.02	S	328.56		
C2An.2n (o)	3.22	81.91	S			84.48	S	80.18					338.78	S	344.32		
C2An.3n (t)	3.33	86.12	S	88.68	S			84.56					367.08	S	372.62		
C2An.3n (o)	3.58			100.99	S			95.49					405.38	S	410.92		
C2Ar-1 (t)	?			—				—					495.93	S	501.47		
C2Ar-1 (o)	?			—				—					501.21	S	506.75		
C3n.1n (t)	4.18			126.20	U			120.70					510.05	S	515.59		
C3n.1n (o)	4.29			135.00	U			129.50					536.53	S	542.07		
C3n.1n-1 (t)	?			136.32	U			131.09					—		—		
C3n.1n-1 (o)	?			136.82	U			131.32					—		—		
C3n.2n (t)	4.48			141.02	S			136.02					553.70	S	559.24		
C3n.2n (o)	4.62			148.47	S			142.97					583.95	S	589.49		
C3n.3n (t)	4.80			150.31	S			144.81									
C3n.3n (o)	4.89			152.22	S			146.72									
C3n.4n (t)	4.98			161.31	S			155.81									
C3n.4n (o)	5.23			177.86	S			172.36									
C3r-1 (t)	?			195.16	S			189.66									
C3r-1 (o)	?			197.16	S			191.66									
C3An.1n (t)	5.894			210.13	S			204.63									
C3An.1n (o)	6.137			224.30	S			218.80									
C3An.2n (t)	6.269			239.46	S			233.96									
C3An.2n (o)	6.567			257.80	S			252.30									
C3Bn (t)	6.935			292.04	S			286.54									
C3Bn (o)	7.091			302.32	S			296.82									
C3Br.1n (t)	7.135			—				—									
C3Br.1n (o)	7.17			—				—									
C3Br.2n (t)	7.341			—				—									
C3Br.2n (o)	7.375			—				—									
C4n.1n (t)	7.432			322.23	S			316.73									
C4n.1n (o)	7.562			325.80	S			320.30									
C4n.2n (t)	7.65			331.61	S			326.11									
C4n.2n (o)	8.072			356.04	S			350.54									
C4r.1n (t)	8.225				S			364.00									
C4r.1n (o)	8.257				S			369.00									
C4r.2r-1 (t)	8.635			399.86	S			394.36									
C4r.2r-1 (o)	8.651			404.85	S			399.35									

Table T7 (continued).

Event	Age (Ma)	Hole 1095A (mbsf)	Sample type	Hole 1095B (mbsf)	Sample type	Hole 1095D (mbsf)	Sample type	Summary (mcd)	Hole 1096A (mbsf)	Sample type	Hole 1096B (mbsf)	Sample type	Hole 1096C (mbsf)	Sample type	Summary (mcd)	Hole 1101A (mbsf)	Sample type
C4An (t)	8.699			411.72	S			406.22									
C4An (o)	9.025			446.00	S			440.50									
C4Ar.1n (t)	9.23			460.87	S			455.37									
C4Ar.1n (o)	9.308			485.53	S			480.03									
C4Ar.2n (t)	9.58			520.50	S			515.00									

Notes: Details are presented in Acton et al. (**Chap. 37,** this volume). Shaded boxes = either an interval drilled but not cored or an interval not drilled. U = U-channel. S = Split-core.

Table T8. Downhole magnetic logging data from the second run of the GHMT logging tool.

Logging Depth (m)	Depth (mbsf)	Depth (mcd)	Total field (nT)	Susceptibility (ppm)	Induced field (nT)	Field anomaly (nT)	Uncorrected remanent anomaly (nT)	Remanent anomaly (nT)
116.637	110.534	105.034	44,129.16	1264.28	77.62	121.98	44.36	85.51
117.551	111.638	106.138	44,030.28	3593.01	118.07	105.63	–12.44	29.11
117.704	111.814	106.314	44,072.57	3637.99	118.71	87.84	–30.87	10.75
118.313	112.512	107.012	44,174.24	3796.99	117.44	68.17	–49.27	–7.38
118.466	112.687	107.187	44,229.93	3274.04	115.62	47.05	–68.57	–26.62
118.618	112.861	107.361	44,203.47	3515.90	113.37	25.58	–87.78	–45.77
118.770	113.036	107.536	44,222.54	3158.72	111.03	3.47	–107.56	–65.48
118.923	113.211	107.711	44,222.90	3290.98	109.03	–19.01	–128.04	–85.89
119.075	113.385	107.885	44,286.82	3222.00	107.56	–41.49	–149.05	–106.84
119.228	113.561	108.061	44,266.46	3256.01	106.75	–63.72	–170.47	–128.19
119.990	114.435	108.935	44,374.56	3521.00	109.19	–83.92	–193.11	–150.49
120.142	114.609	109.109	44,403.61	3519.99	108.85	–99.29	–208.14	–165.46
120.294	114.783	109.283	44,390.74	3336.23	107.67	–107.30	–214.98	–172.23
120.447	114.959	109.459	44,397.80	3196.98	105.67	–107.45	–213.12	–170.31
121.361	116.006	110.506	44,338.10	2889.00	84.95	–100.86	–185.81	–142.60
121.666	116.356	110.856	44,404.64	2136.09	67.76	–89.47	–157.22	–113.87
121.818	116.530	111.030	44,344.66	1041.00	58.34	–75.89	–134.23	–90.81
121.971	116.706	111.206	44,343.56	939.97	49.75	–62.50	–112.25	–68.77
122.123	116.880	111.380	44,337.72	1072.04	42.85	–50.36	–93.21	–49.66
122.276	117.056	111.556	44,321.06	1251.00	38.10	–40.50	–78.60	–34.99
122.428	117.230	111.730	44,310.59	1211.98	35.42	–33.96	–69.39	–25.70
122.580	117.404	111.904	44,310.04	942.97	34.13	–32.02	–66.15	–22.40
122.733	117.580	112.080	44,310.85	860.03	33.39	–34.29	–67.68	–23.86
122.885	117.754	112.254	44,324.15	1013.00	33.04	–38.36	–71.40	–27.51
123.038	117.929	112.429	44,352.72	902.00	33.43	–42.53	–75.95	–32.01
123.190	118.104	112.604	44,371.59	1168.04	34.78	–45.55	–80.33	–36.31
123.342	118.278	112.778	44,390.60	807.08	36.82	–46.66	–83.47	–39.39
123.647	118.628	113.128	44,324.61	1191.07	40.77	–45.84	–86.61	–42.40
123.800	118.797	113.297	44,318.44,	1813.96	41.89	–43.70	–85.59	–41.31
123.952	118.925	113.425	44,366.79	941.03	42.38	–41.08	–83.46	–39.11
124.104	119.054	113.554	44,356.72	1319.99	42.38	–39.17	–81.54	–37.13
124.257	119.183	113.683	44,356.44,	1194.00	42.17	–39.45	–81.61	–37.13
124.409	119.312	113.812	44,353.69	1200.03	42.25	–43.16	–85.41	–40.87
124.562	119.441	113.941	44,350.97	1353.00	43.09	–50.25	–93.35	–48.73
124.714	119.570	114.070	44,344.15	1348.00	44.93	–60.58	–105.51	–60.83
124.866	119.698	114.198	44,385.13	1360.01	47.99	–74.60	–122.59	–77.84
126.086	120.730	115.230	44,438.54	3044.00	101.56	–91.07	–192.63	–147.34
126.238	120.859	115.359	44,476.16	3266.04	105.29	–107.01	–212.31	–166.96
126.390	120.987	115.487	44,440.90	3469.01	107.26	–118.98	–226.24	–180.83
126.543	121.117	115.617	44,499.91	3586.02	107.43	–124.17	–231.60	–186.12
126.695	121.245	115.745	44,498.59	3424.96	105.83	–121.57	–227.41	–181.86
129.743	123.823	118.323	44,501.73	2468.95	98.34	–112.40	–210.74	–163.86
129.896	123.952	118.452	44,468.07	2019.00	99.46	–99.20	–198.67	–151.72
130.048	124.081	118.581	44,433.72	2458.14	104.03	–84.59	–188.62	–141.61
130.200	124.209	118.709	44,426.34	3900.22	109.37	–70.63	–179.99	–132.91
130.353	124.339	118.839	44,426.45	5296.98	112.08	–59.74	–171.82	–124.67
130.505	124.467	118.967	44,425.79	4530.74	109.60	–53.43	–163.03	–115.81
130.658	124.623	119.123	44,421.99	2816.12	101.02	–50.99	–152.01	–104.73
130.810	124.782	119.282	44,416.49	1996.94	87.41	–50.87	–138.28	–90.94
130.962	124.940	119.440	44,418.07	1789.98	71.24	–51.54	–122.78	–75.37
131.267	125.257	119.757	44,465.27	830.03	43.08	–51.32	–94.40	–46.85
131.420	125.416	119.916	44,434.70	1092.01	34.26	–48.48	–82.74	–35.13

Notes: The logging depths for the second run of the GHMT logging tool are converted to mcd and mbsf depth scales using linear interpolation between the tie points from Table **T16,** p. 61, of Acton et al. (**Chap. 37,** this volume). Total field = the total magnetic field measured downhole by the GHMT logging tool. Susceptibility = the susceptibility measured downhole by the GHMT logging tool. Induced field = the field anomaly in the borehole caused by the induced magnetization of the sediment; calculated from the susceptibility log. Field anomaly = total field minus the International Geomagnetic Reference Field and the field due to the drill pipe; it is calculated from the total field and includes the remanent and induced borehole field anomalies (Williams et al., **Chap. 31,** this volume). Uncorrected remanent anomaly = the field anomaly in the borehole caused by the remanent magnetization of the sediment. Remanent anomaly = the uncorrected remanent anomaly minus a linear downhole trend (Williams et al., **Chap. 31,** this volume). Only a portion of this table appears here. The complete table is available in **ASCII format**.